

DYNAMIC INSTABILITY AND "BUZZ"  
AT AIR TURNING BARS

By

LINDA LEI CHEN

Bachelor of Science

China Textile University

Shanghai, China

1991

Submitted to the Faculty of the  
Graduate College of the  
Oklahoma State University  
in partial fulfillment of  
the requirements for  
the Degree of  
MASTER OF SCIENCE  
May, 1996

DYNAMIC INSTABILITY AND "BUZZ"

AT AIR TURNING BARS

Thesis Approved:

*Paul W. Mowbray*

Thesis Adviser

*B. E. Jones*

*[Signature]*

Thomas C. Collins  
Dean of the Graduate College

---

## ACKNOWLEDGMENT

I would like to express my deepest gratitude and respect towards my advisor, Dr. P.M. Moretti, for his excellence in guiding and encouraging me. I thank him for his patience and timely suggestions. I would also like to thank Dr. Y.B. Chang for his constant help and suggestions throughout the completion of this project. I like to thank Dr. Price and Dr. Chambers for serving on my graduate committee.

I take this opportunity to express my appreciation to my parents and sister, whose love and encouragement supported me during the study.

This work was supported by the Web Handling Research Center (WHRC) at Oklahoma State University.

## TABLE OF CONTENTS

Chapter	Page
I. INTRODUCTION . . . . .	1
1.1 Problem Description . . . . .	1
1.2 Objectives. . . . .	3
II. LITERATURE REVIEW . . . . .	4
III. PREVIOUS WORK ON OUT-OF-PLANE INSTABILITIES . . . . .	11
3.1 Five Types of Out-of-Plane Instabilities . . . . .	11
3.2 Maps of Out-of-Plane Flutter . . . . .	22
IV. FREE-SPAN FLUTTER . . . . .	27
4.1 Experimental Setup . . . . .	27
4.2 Results and Discussions. . . . .	31
4.21 Free-Span Flutter with No Edge Air Leakage . . . . .	32
4.22 Free-Span Flutter with Edge Air Leakage . . . . .	42
V. NONDIMENSIONAL PARAMETERS . . . . .	59
5.1 Introduction of $\pi$ Theorem. . . . .	59
5.2 Nondimensional Parameters . . . . .	60
VI. SUMMARY AND CONCLUSIONS . . . . .	73
REFERENCES . . . . .	75
APPENDIX: TRAVELING WAVE ANALYSIS . . . . .	77

## LIST OF TABLES

Table	Page
Table 4.1 Data of Frequency and Amplitude (No Air Leakage) . . . . .	40
Table 4.2 Effect of Wrap Angle with Big Gap. . . . .	44
Table 4.3 Wrap Angles with Different Modes . . . . .	47
Table 5.1 List of Variables and Dimensions . . . . .	61

## LIST OF FIGURES

Figure	Page
Figure 2.1 Schematic of Air Turning Bar and Web . . . . .	5
Figure 2.2 Segawa's Model . . . . .	7
Figure 3.1 Tested Air Bars. . . . .	12
Figure 3.2 Touching of Web to the Air Turning Bar . . . . .	14
Figure 3.3 Free-Span Flutter . . . . .	16
Figure 3.4 Bumping of the Web . . . . .	18
Figure 3.5 In-Phase Flutter . . . . .	19
Figure 3.6 Bulging of the Web . . . . .	21
Figure 3.7 Effect of Tension Parameter at Air Turning Bar with Two Rows of Holes . . . . .	24
Figure 3.8 Effect of Tension Parameter at Air Turning Bar with Multiple Rows of Holes . . . . .	26
Figure 4.1 Schematic of Air Turning Bar and Web Setup . . . . .	29
Figure 4.2 Schematic of Measuring Equipment Setup . . . . .	30
Figure 4.3 Effect of Web Tension on Flutter Frequency . . . . .	37
Figure 4.4 Effect of Tension Parameter on Flutter Frequency . . . . .	38
Figure 4.5 Effect of Tension Parameter on Flutter Amplitude . . . . .	39

---

Figure	Page
Figure 4.6 Spectrum Plot (No Air Leakage) . . . . .	41
Figure 4.7 Different Modes . . . . .	45
Figure 4.8 Effect of Tension Parameter on Flutter Amplitude and Frequency . . . . .	50
Figure 4.9 Effect of Pressure on Flutter Frequency . . . . .	52
Figure 4.10 Effect of Pressure on Flutter Amplitude . . . . .	53
Figure 4.11 Effect of Web Tension and Length on Flutter Frequency . . . . .	55
Figure 4.12 Effect of Length Parameter on Flutter Frequency . . . . .	56
Figure 4.13 Phase Shift . . . . .	58

## NOMENCLATURE

a	Amplitude
C	Wave speed
d	Diameter of the air bar
D	Stiffness of web per unit width
f	Vibration frequency
h	Flotation height of web
k	Wave number
L	Web length
m	Mass per unit width
$P_0$	Supply pressure
P	Pressure
Q	Volume flow rate per unit width
t	Time
T	Tension per unit width
$U_{0c}$	Critical stable flow velocity of the antiwall side flow
$U_c$	Critical flow velocity of the wall side flow
$\alpha$	Half of the angle covered by the outermost rows of holes



$\beta$	Half of the wrap angle
$\theta$	Wrap Angle ( $\alpha-\beta$ ), equals negative overlap angle
$\gamma$	Mass density of web
$\lambda$	Wavelength
$\mu$	$x/l$
$\nu$	Kinematics viscosity
$\rho$	Density of air
$\rho_0$	Density of initial air

## CHAPTER I

### INTRODUCTION

#### 1.1 Problem Description

A thin and flexible material, such as paper, plastic sheet, polymer film, and magnetic media, manufactured in continuous form, is called web. Web is transported under tension through various processes such as printing, drying, coating, laminating etc. prior to being converted to a final product. Airbars are used to support the moving during the drying of the coated or printed polymers, because the coated side of the web can not be touched until it is dry. The air moving over the wet side of the web can also reduce the drying time. This drying phenomenon combined with aerodynamic support is called web flotation drying, where jets of air support a thin moving web, without mechanical contact, and dry the surface coatings. The nozzles that apply air to the web are called airbars.

Air-turning bars are another kind of no-contact support device. They are used mainly to change the direction of motion of a web. Air-turning bars are designed to avoid web contact with solid surfaces, to provide uniform and controlled heat and mass transfer, to avoid flow instabilities regardless of web tension, and to provide simplicity of operation.

When air bars are used in the handling of webs, a variety of instability problems can occur. Lateral instability and wrinkling are the most serious problems. Under some

operating conditions, high-frequency flutter or “buzz” occurs, resulting in damage to the webs and coatings. This problem causes waste of time and material. The purpose of this study is to investigate this dynamic problem, finding out what causes the problem so it will be possible to avoid this kind of problems in industrial applications.

The following assumptions are made in this study:

1. The flow is two-dimensional and incompressible.
2. The membrane deflection is negligibly small compared to its length.
3. The inclination of the wall is small.
4. The flow is irrotational (or potential).
5. The flow velocity and density in the flow partitioned by the membrane are uniform.

Side plates were used in some tests to reduce air loss from the edges of the web to simulate very wide webs. The amount of the side leakage of air was controlled by changing the gaps between the web and the side plates.

## 1.2 Objectives

In a previous study by Zeelani (1994), five types instabilities of out-of-plane flutter were identified, including three dynamic and two static instabilities. He determined the parameter maps of the operating conditions of the instabilities, except for free-span flutter. My tests focus on free-span flutter, with a purpose of determining the effects of web tension, supply air pressure, free-span length, and wrap angle. Using existing wave theory, motion of free-span flutter is examined. Non-dimensional parameters are found for non-dimensional analysis.

A traveling-wave experimental theory related with the current study is re-examined. Also, non-dimensional parameters for free-span flutter are discussed.

## CHAPTER II

### LITERATURE REVIEW

It is found that very few articles discuss air turning bars. Fraser (1983) gives some basic ideas about useful devices for non-touching support of webs. He describes two typical patterns of air-emitting nozzles: slots and holes. One problem with air-turning bars is that there is excessive air loss through the slot areas which are not covered by the web. By mounting side plates adjusted to the width of the web, we can minimize the air loss from the edges of the web. It could cause another problem, though, in that the soft edge of the web could be damaged if the plates are not well adjusted. A practical design of air turning bars is to countersink holes on the surface. A schematic drawing of the air turning bar and the web is shown in Figure 2.1.

Several papers discuss some specific hydrodynamics of liquid-structure interaction phenomena occurring at the air turning bars. The related critical equations of the flow for plastic web are discussed in this chapter.

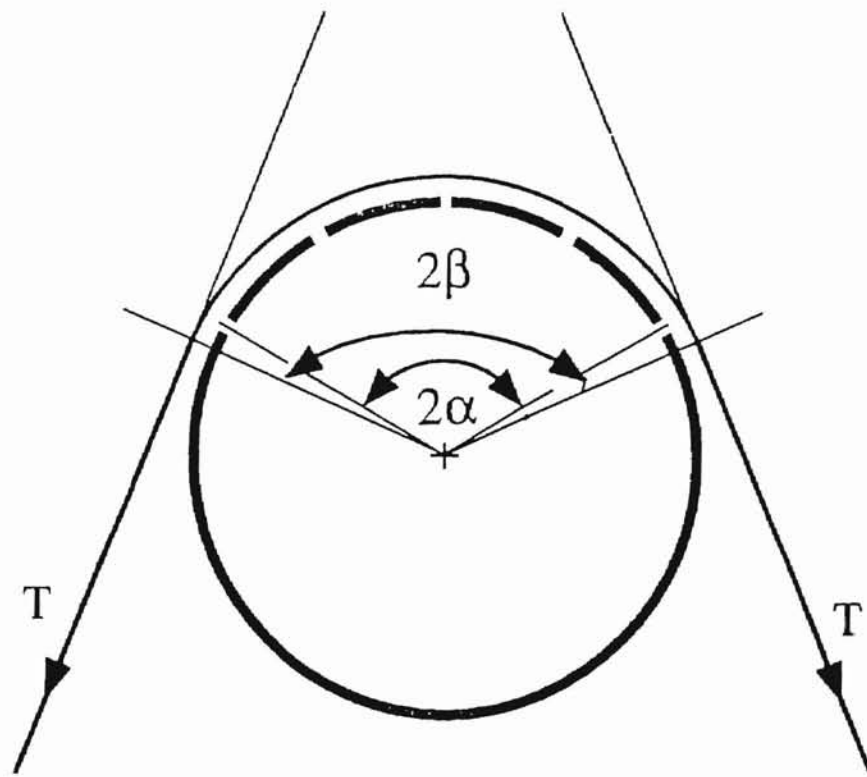


Figure 2.1 Schematic of Air Turning Bar and Web

## Web Instability due to Channel Flow

According to Sundararajan (1966) and Segawa (1993), a flexible web placed adjacent to a rigid wall can experience instability due to the air flowing through the gap between the web and the wall. Segawa's research showed the destabilizing effect of a rigid wall on the elastic one-dimensional flat plate placed in irrational flows adjoining the rigid wall (in Figure 2.2). This instability phenomenon is sensitive to the inclination angle and the distance between the web and the wall. At the air turning bars, the air flowing through the gap along the web surfaces can cause the same kind of instability.

### Flow instability

When the area of the flow path suddenly increases, the air flow may separate from either boundary. According to Moretti (1990), in many cases the flow stream deflects toward one side or the other, and in some cases it oscillates and causes pressure fluctuations on the flow boundary. Flow instability around air flotation bars was demonstrated on a water table in Purdue's report (1993). The same phenomenon can occur on air turning bars, because the flow paths expand suddenly near the points where the web leaves the air turning bars. According to Aidun (1991), a variety of flow instability phenomenon may occur in various web handling processes.

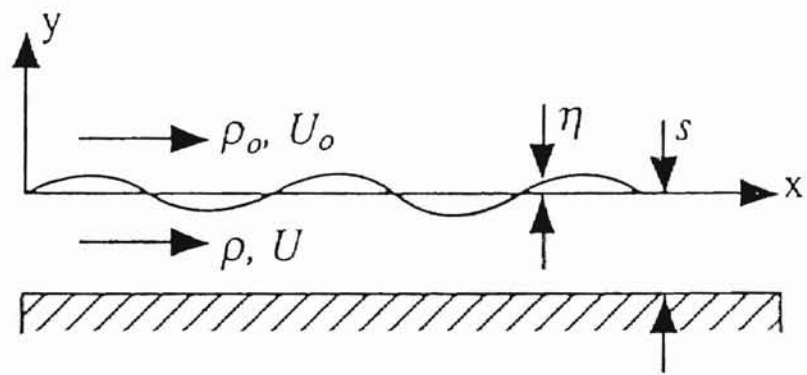


Figure 2.2 Segawa's Model



In Sundararajan's model, he assumes that the air on the top of the membrane is still. The critical flutter speed of a given mode is its wave speed in still air, and it increases with decreasing wave length. The wave length and wave pattern are also important factors. In his study, the aerodynamic instability of an infinitely long membrane that is parallel to a rigid wall is discussed. The flow between the membrane and the wall is considered two-dimensional, incompressible and subsonic. Sundararajan's model is very close to Segawa's (shown in Figure 2.3) except that the flow velocity and the fluid density of the antiwall side flow are assumed to be zero. So, Segawa's characteristic equation is considered more general, because he included the flow velocity of the antiwall side flow  $U_0$  and the fluid density of the antiwall side flow  $\rho_0$ .

According to Segawa, the characteristic equations of the one-dimensional flat plate (membrane in Sundararajan's model) placed parallel to the uniform flow adjoining the rigid flat wall are:

$$U_{0c} = \sqrt{\delta(1 + \mu + \nu)}; \quad (2.1)$$

$$U_c = \sqrt{\delta\left(1 + \mu + \frac{1}{\nu}\right)}. \quad (2.2)$$

$$\delta = \frac{Dk^4 - (p_0 - \rho)g}{\mu\rho_m hk^2}, \quad \mu = \frac{\rho_t}{\rho_m hk}, \quad \nu = \frac{C\rho}{\rho_0}$$

where  $U_{0c}$  is the critical flow velocity of the antiwall side flow,  $U_c$  is the critical flow velocity of the wall side flow.

We can apply Segawa's and Sundararajan's models to obtain the stability criteria (detail in Appendix B) for a web. The stability criterion for a taut web is

$$U_{air}^2 = \frac{T}{m} \left(1 + \frac{4\pi^2 D}{T\lambda^2}\right) \left(1 + \frac{2\pi m}{\rho\lambda} \tanh\left(\frac{2\pi h}{\lambda}\right)\right) \quad (2.3)$$

The stability criterion for a slack web is

$$U_{air}^2 = \frac{4\pi^2 D}{T\lambda^2} \left(1 + \frac{2\pi m}{\rho\lambda} \tanh\left(\frac{2\pi h}{\lambda}\right)\right) \quad (2.4)$$

where  $U_{air}$  is the critical flow velocity of the wall side flow,  $T$  is tension,  $m$  is mass per unit area,  $D$  is bending stiffness of the web,  $\lambda$  is wavelength,  $h$  is flotation height (distance between the web and the solid wall, and  $\rho$  is fluid density of the wall side flow. The critical flow velocity monotonically increases with the spacing between the web and the wall, and decreases with the increase of wavelength.

If we consider a stationary membrane neglecting the air inertia, the natural frequency increases when tension increases and it decreases when length increases.

$$f_n = \frac{nc}{2L} = \frac{n}{2L} \sqrt{\frac{T}{m}} \quad (2.5)$$

where  $n$  is the order of mode,  $L$  is the length of the web,  $T$  is tension, and  $m$  is mass per unit length.

## CHAPTER III

### PREVIOUS WORK ON OUT-OF-PLANE INSTABILITIES

#### 3.1 Five Types of Out-of-Plane Instabilities

In Zeelani's exploratory experiment (1994), two types of air turning bars have been used, as shown in Figure 3.1. Both bars have a length of 6 inches and a diameter of 2 inches. One has many rows of holes while the other has two rows of holes. For the simplicity of tests, the web was mounted asymmetrically as shown in Figure 3.2. With this setup, the wrap angle can be changed by turning the air.

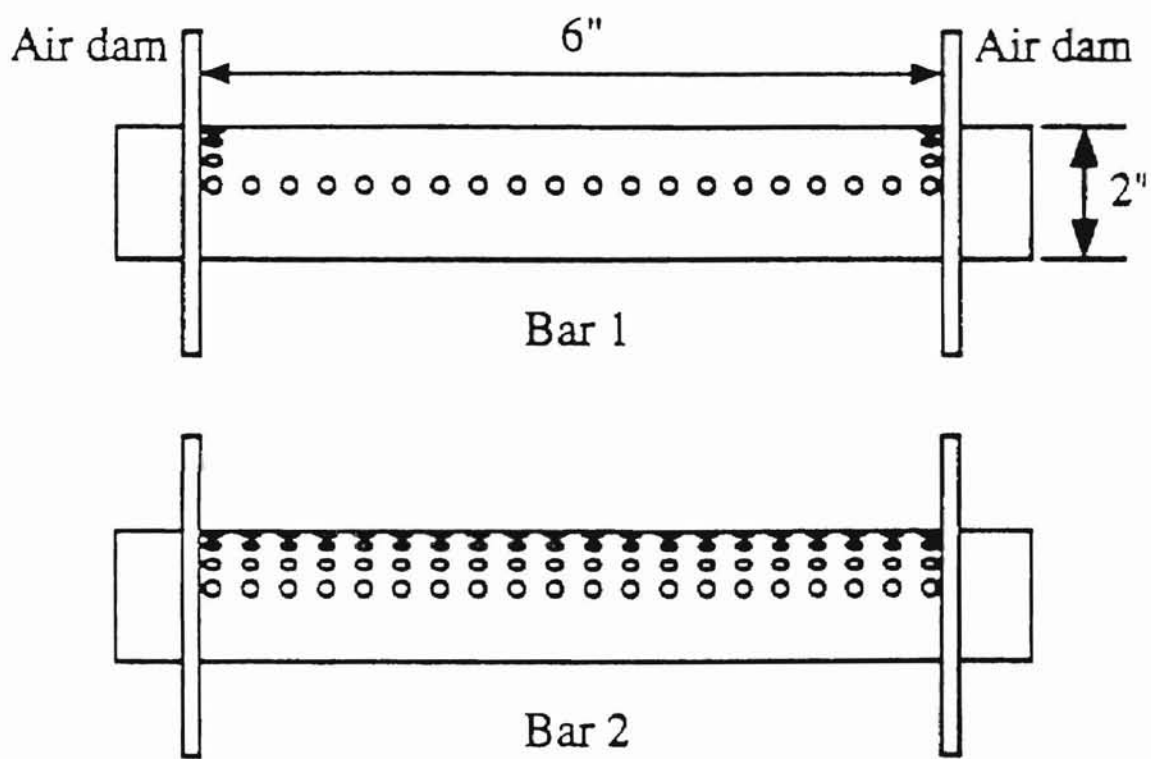


Figure 3.1 Tested Air Bars

Five types of phenomena, including three types of dynamic instabilities, were observed under different operation conditions by changing the supply air pressure, the tension, or the wrap angles in Zeelani's experiments (1994).

#### Touching of the Web to the Air Turning Bar

The static instability of the touching of the web to the air turning bar occurs if the web tension is too high or the supply pressure is too low. As mentioned earlier, the air jet from the air turning bar should support the web without mechanical contact. If the tension is too high, compared to the supply pressure, or the supply pressure is too low, the air jet will not be strong enough to support the web. Thus, the web would lie on the air turning bar, as shown in Figure 3.2. Practical operating conditions should have tensions less than this extreme condition, or the supply pressure should be above this extreme condition. Once the supply pressure overcomes the tension induced pressure, the web will float again.

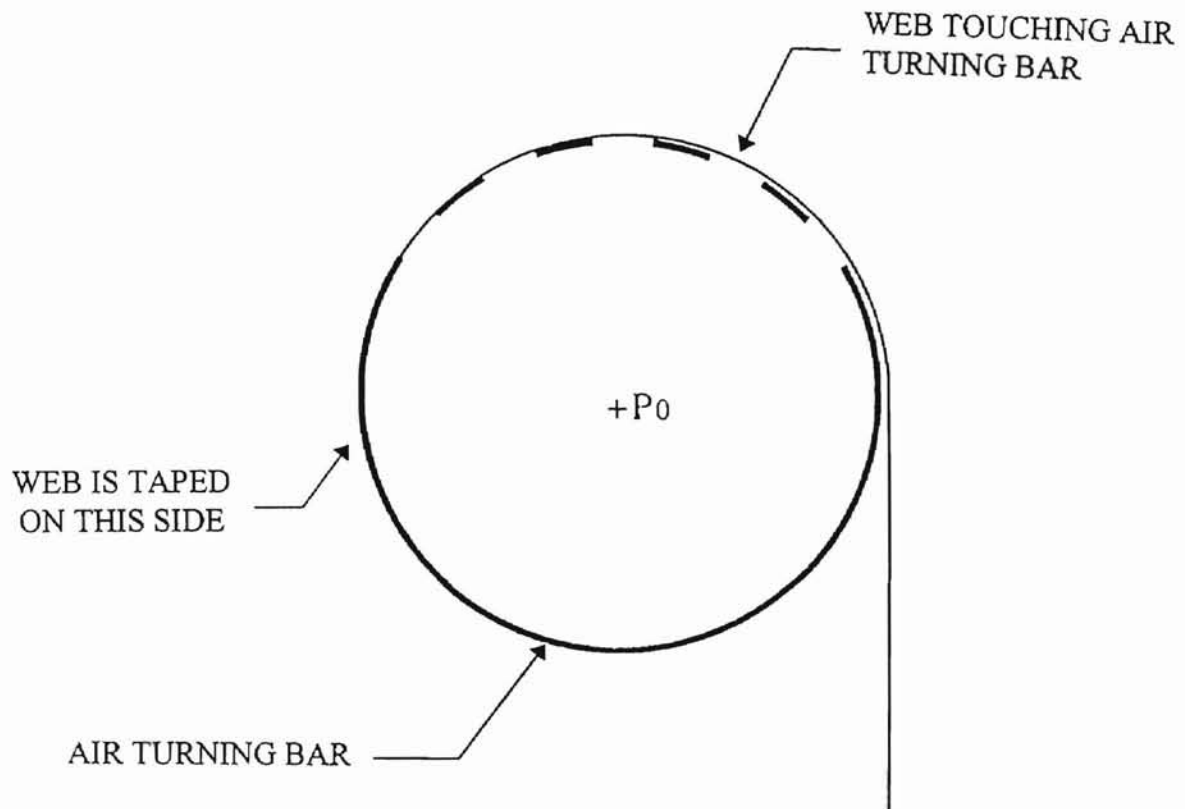


Figure 3.2 Touching of Web to the Air Turning Bar

### Free-Span Flutter

The dynamic instability of free-span flutter will be discussed in further detail in Chapter IV. At some operating conditions, the web span between the air turning bar and the adjacent support vibrates severely at its fundamental mode causing loud noises. When this happens, the floating central region of the web is almost stable and there is no height fluctuation as shown in Figure 3.3. This type of instability occurs over a wide range of wrap angle. The web frequency increased when the tension increased or the web span decreased. The gap between the side plate and the edge of the web can affect the vibration mode of the web.

This type of instability could be caused by one or more of the three causes: parallel channel flow, diverging channel flow, and wall jet.



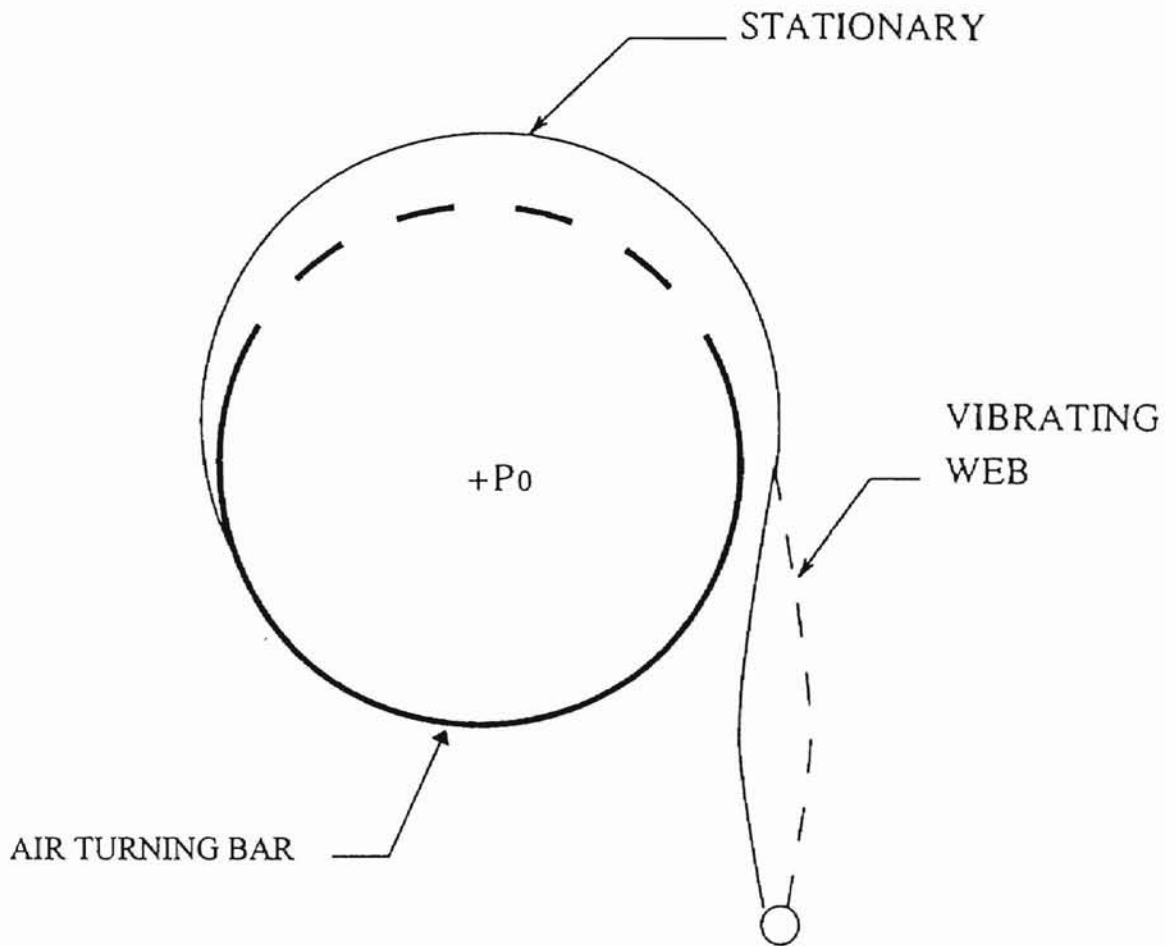


Figure 3.3 Free-Span Flutter

### Bumping of the Web (Out-of-Phase Flutter)

Bumping of the web, also called the out-of-phase flutter, is shown in Figure 3.4. This type of dynamic instability occurs only when the outer row of holes is located near the tangential contact line. The web span between the air turning bar and the support vibrates out-of-phase with that portion of the web that wraps the air turning bar. The web experiences a large amplitude of “bumping” motion. The flotation height of the web fluctuates with constant frequency. The role of the air jet near the tangential line seems critical in this type of instability.

One of the possible causes of the out-of-phase flutter might be the ground effect. According to the ground effect theory (Banks, 1988), the angle of the air jet is one of the dominating factors for the air pressure developed in the region surrounded by the jets.

Out-of-phase flutter can be avoided if the outer row of holes is away from the tangential line. This type of flutter can also be alleviated by increasing the web tension.

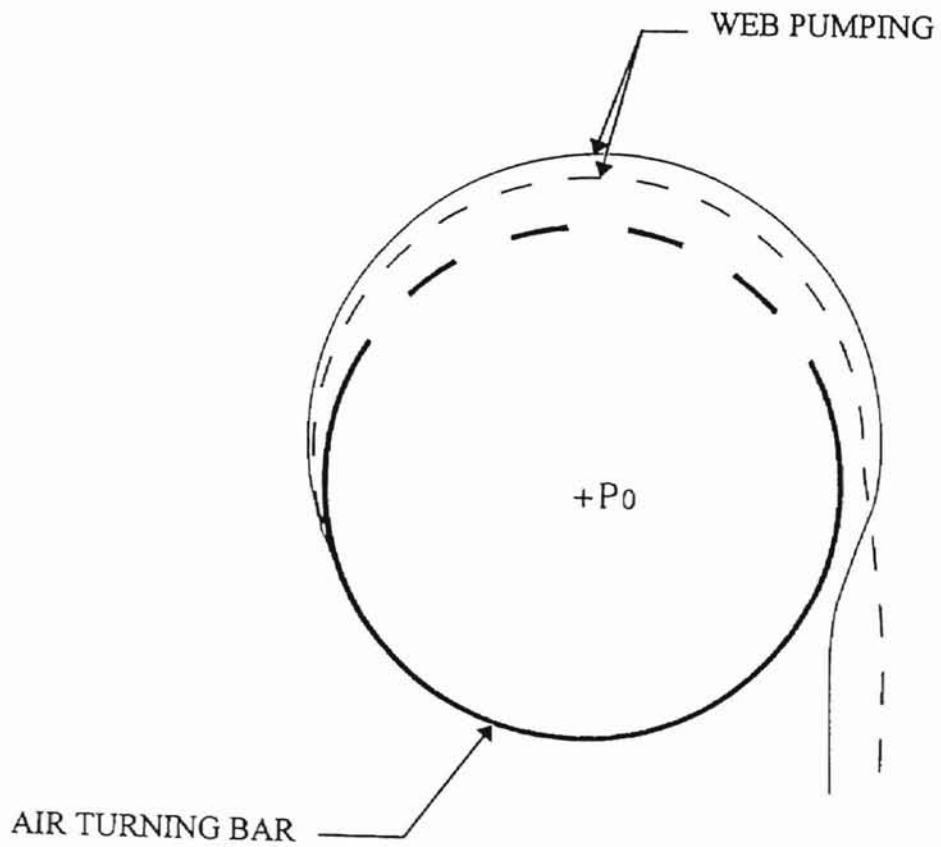


Figure 3.4 Bumping of the Web

### In-Phase Flutter

The instability caused by in-phase flutter happens under some operation conditions. It appeared to be floating, but actually the part of the web which covered the air turning bar was vibrating with small amplitudes. It is shown in Figure 3.5.

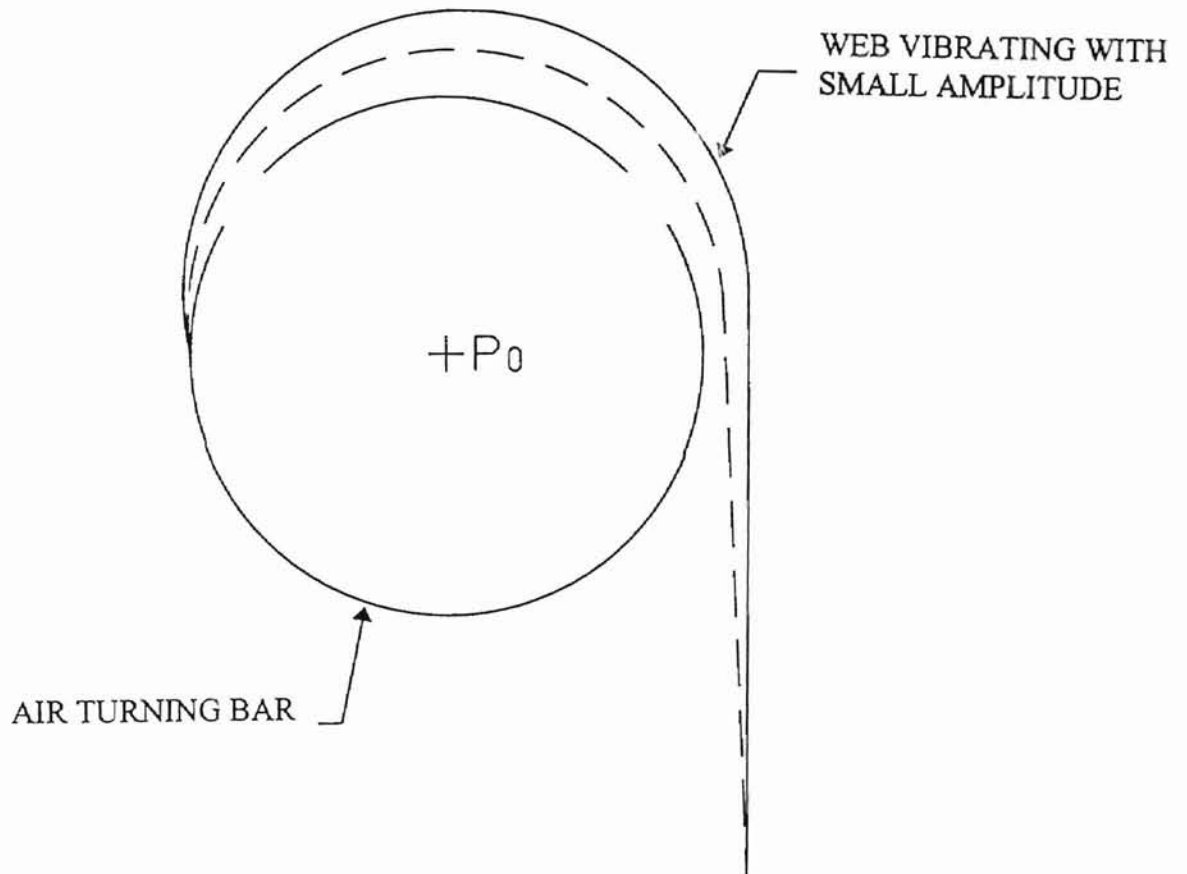


Figure 3.5 In-Phase Flutter

### Bulging of the Web

Bulging of the web (or called free float) occurs when the web tension is too low or the supply pressure is too high. It is a non-oscillatory phenomenon as shown in Figure 3.6. When the supply pressure is high and the pressure drop across the holes is not high enough, the pressure developed in the gap between the web and the air turning bar is larger than the tension induced pressure. Thus, the web cannot find its equilibrium position near the tube surface. The air gap in the control region of the floating web becomes excessively large and most of the air escapes through the edges of the web. When end plates are mounted to prevent side leakage, the air gap of the center part can increase until the web deflects beyond the edges of the end plates.

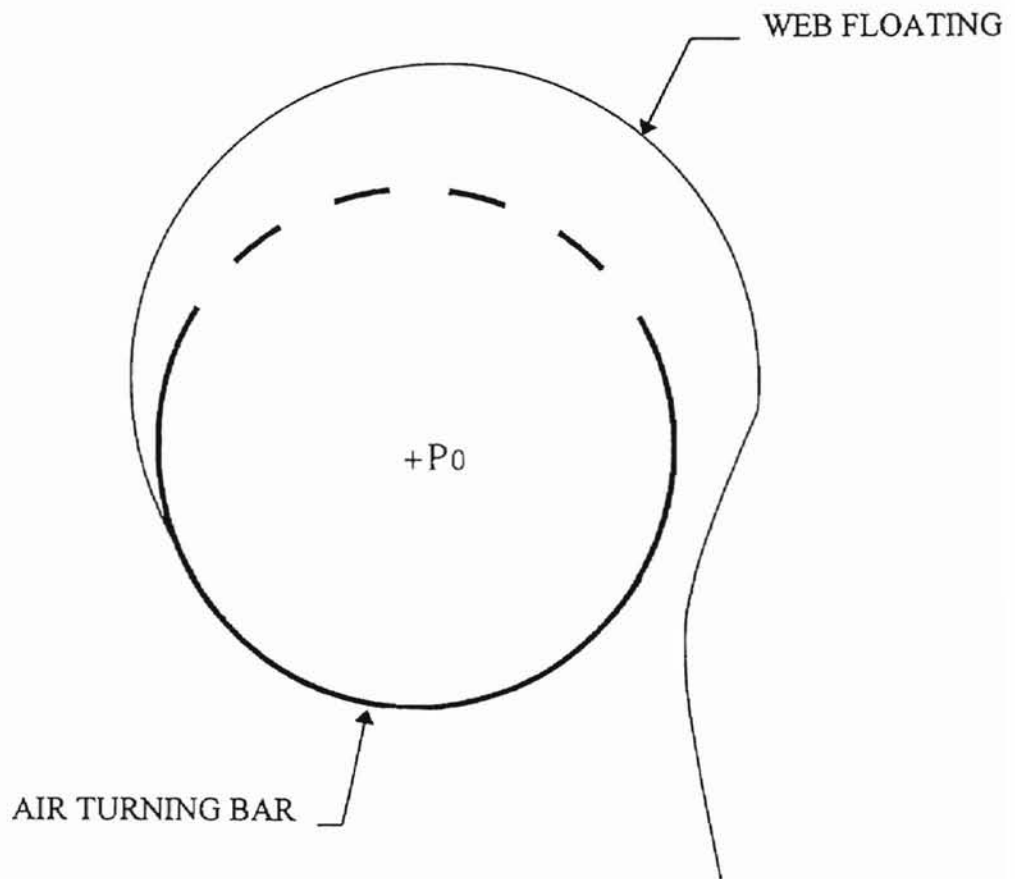


Figure 3.6 Bulging of the Web

## 3.2 Maps of Out-of-Plane Flutter

Two maps are used here to illustrate the conditions where four instabilities happened. The four phenomena discussed here are: (1) touching of the air turn bar, (2) in phase flutter, (3) bumping of the web, and (4) bulging of the web (or free float). Free-span flutter is detailed in Chapter IV. Figure 3.7 shows that the test results for the air bar having two rows of holes, while Figure 3.8 is for the air bar with a dense array of holes.

### Effect of Tension Parameter at Air Turning Bar with Two Rows of Holes

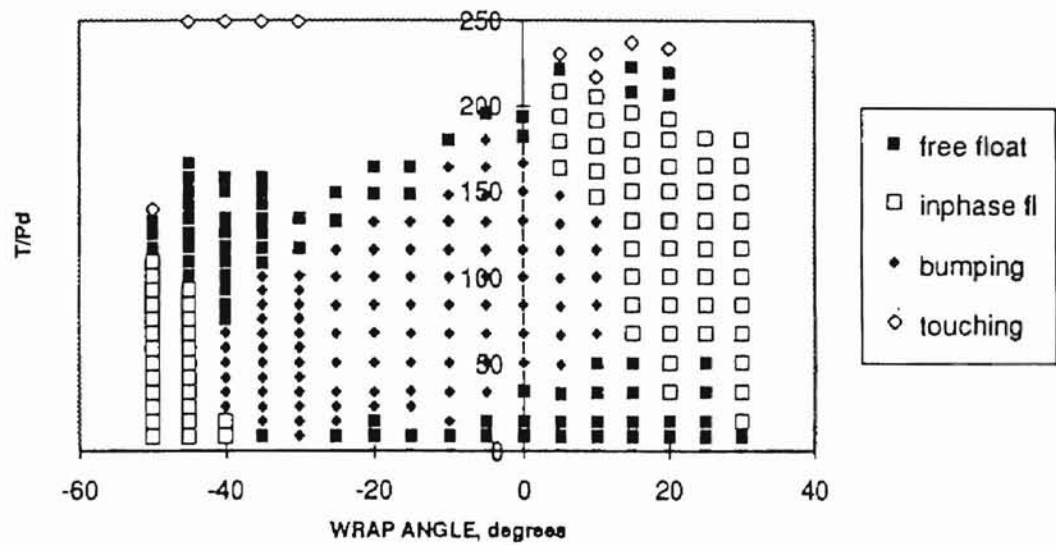
Figure 3.7 shows the effects of the wrap angle  $\theta$  ( $\theta = \alpha - \beta$ , which is a negative overlap angle) and the tension parameter. For example, at -50 degrees, low in-phase flutter is observed at low "T/Pd" (T is tension per unit width, P is supply pressure, d is diameter of air turn bar, detail of T/Pd discussed in section 5.2). Above a particular value of "T/Pd", in this case 110, there is almost no flutter and the web seems to float freely without touching the air turning bar. At values of "T/Pd" above 140, the web touches the air turning bar.

At wrap angles starting from -40 degrees bumping of the web begins. At this wrap angle, bumping of the web starts at a "T/Pd" value of 20. Below this value there is low in-phase flutter. Bumping of the web occurs up to a "T/Pd" value of 77. Above this value, the web seems to float freely without touching the air turning bar. Once the "T/Pd" value increases above 250, the web touches the air turning bar. When wrap angle is close to zero, bumping of the web becomes more violent. The range of wrap angles at which the bumping of the web occurs is -40 to 15 degrees for 2-inch diameter air turning bar. At a

wrap angle of 15 degrees and above, there is no bumping of the web. At low value of “ $T/Pd$ ”, from 0 to 50, the web floats freely without touching the air turning bar. As the “ $T/Pd$ ” value increases above 50, a weak in-phase flutter appears. The in-phase flutter is observed until the value of  $T/Pd$  reaches 200. Above this value the web floats freely up to a value of 225. When  $T/Pd$  exceeds 225, the web touches the bar.



EFFECT OF T/Pd FOR AIRBAR WITH TWO ARRAYS OF HOLES



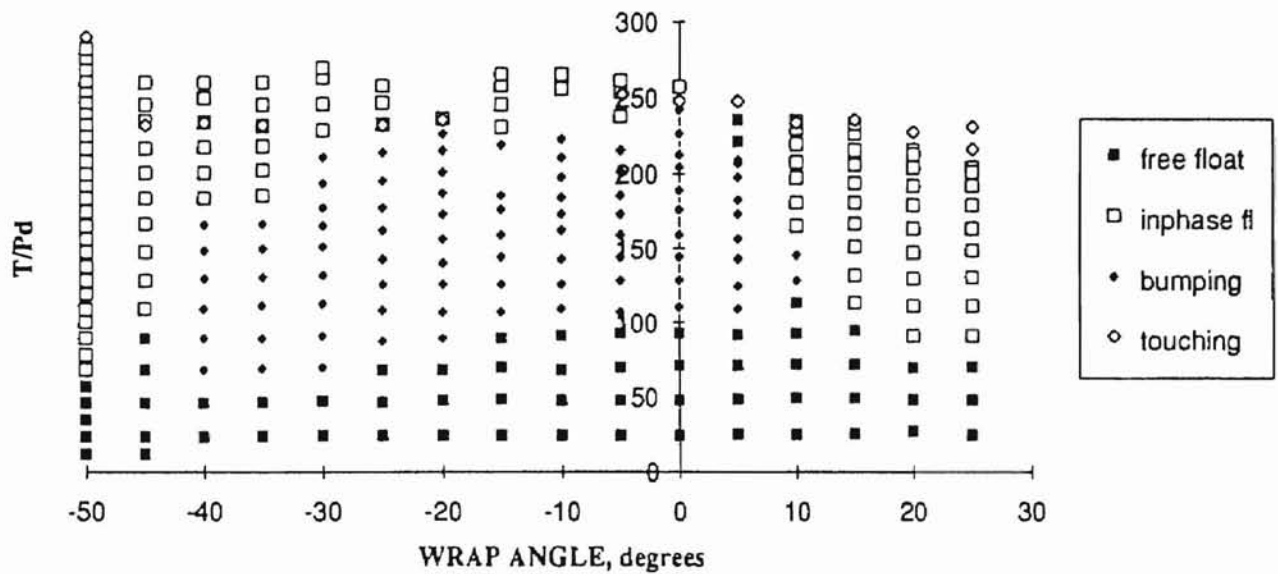
- T/Pd -- T is tension per unit width, P is supply pressure, d is diameter of air turning bar
- wrap angle --  $\theta$  ( $\alpha - \beta$ )

Figure 3.7 Effect of Tension Parameter at Air Turning Bar with Two Rows of Holes

### Effect of Tension Parameter at Air Turning Bar with Multiple Rows of Holes

From Figure 3.8, we can see that the range of wrap angles at which bumping occurs is from -40 to 15 degrees. This is the same as that of the air turning bar with two rows of holes except that the bumping occurs over comparatively larger range of wrap angles. When the last row of holes is away from the tangential line of the web, for example -40 degrees, the web floats freely at low "T/Pd" value. At 50 and above, there is in-phase flutter. Above 250 the web touches the air turning bar. Similarly from -40 degrees to 10 degrees, the web floats freely at low "T/Pd" values. In the same range of wrap angle, if the "T/Pd" value is roughly 75 to 220 then bumping occurs (as shown in Figure 3.8). When "T/Pd" is greater than 230, the web touches the air turning bar for all wrap angles from -50 to 30 degrees. For all wrap angles, the web floats freely at low "T/Pd" values. Above 10 degrees of wrap angle and "T/Pd" roughly between 100 to 220, in-phase flutter starts. In-phase flutter occurs also in the range of -50 to 0 degrees and "T/Pd" values climbing on a curve from 70 to 250. At very high "T/Pd" values the web touches the air turning bar.

### EFFECT OF T/Pd FOR AIRBAR WITH DENSE ARRAY OF HOLES



- T/Pd -- T is tension per unit width, P is supply pressure, d is diameter of air turning bar
- wrap angle --  $\theta$  ( $\alpha$ - $\beta$ )

Figure 3.8 Effect of Tension Parameter at Air Turning Bar with Multiple Rows of Holes

## CHAPTER IV

### FREE-SPAN FLUTTER

#### 4.1 Experimental Setup

The setup of the web and the air turning bar is shown in Figure 4.1. One side of the air turning bar was connected to the blower (a vacuum cleaner with a capacity of 580 cfm at zero pressure load) for the supply of air. The other side of it was connected to a manometer (using 0.826 SP. GR. Red Oil) by which the air pressure was measured in inches of water. One end of the web was sealed to the air bar. Two thin clamping plates were placed at the other end in order to apply a uniform tension to the web. A steel bar was placed between the air turning bar and the clamp to adjust the length of the free span of the web. The angle  $\alpha$ , defined in Figure 2.2, was changed by rotating the air turning bar, and read from the protractors on the side plates.

Two laser Doppler vibrometers were used to measure the wave properties of web flutter along the flow direction. Each laser-Doppler vibrometer consists of two components, Sensor Head (Polytec OFV 350) and Vibrometer Controller (Polytec OFV 2600). The signals from the vibrometers were filtered by low pass filters (Active Filter, Model AF-120). A Signal Analyzer (HP35665) was used to sample and analyze the signals from the low pass filters. The schematic of this measuring setup is shown in Figure 4.2.

The frequency setting on the Signal Analyzer depended on the frequency range of the signals received from the laser Doppler systems. Generally, the range of the low pass filter was set below 200 Hz, because all fundamental frequencies found in the tests were below 200 Hz. Moreover, if the frequency in one test was about 50 Hz, the low-pass filter was set at 60 Hz.

Typically, the frequency range of signal analyzer was set at 200 Hz. Every reading of the frequency and amplitude was an average of 30 samples. The frequency and amplitude were read directly from the signal analyzer. The amplitude was converted from voltage to velocity by using equation (4.1). More detail will be given in section 4.2.

$$A = a * a / 125 \quad (4.1)$$

where A is vibration amplitude (m/s), a is signal amplitude read from signal analyzer, ( $V_{rms}^2$ ), and 125 is a proportionality constant for the laser-Doppler signal level which is from the relationship 1 volt = 1/125 m/s.

One of the vibrometer measurement locations was at about the middle of the span. At the beginning of the test, we found the amplitude was most visible at the middle of the span, but similar results were obtained at other measurement locations. Amplitudes were not reproducible, but the frequency and the trends of amplitude change were same at all test location. For different flutter modes, the first test point was fixed at the location where the most visible amplitude appeared, and the second measurement location was moved along the span to see the phase shift of the wave.

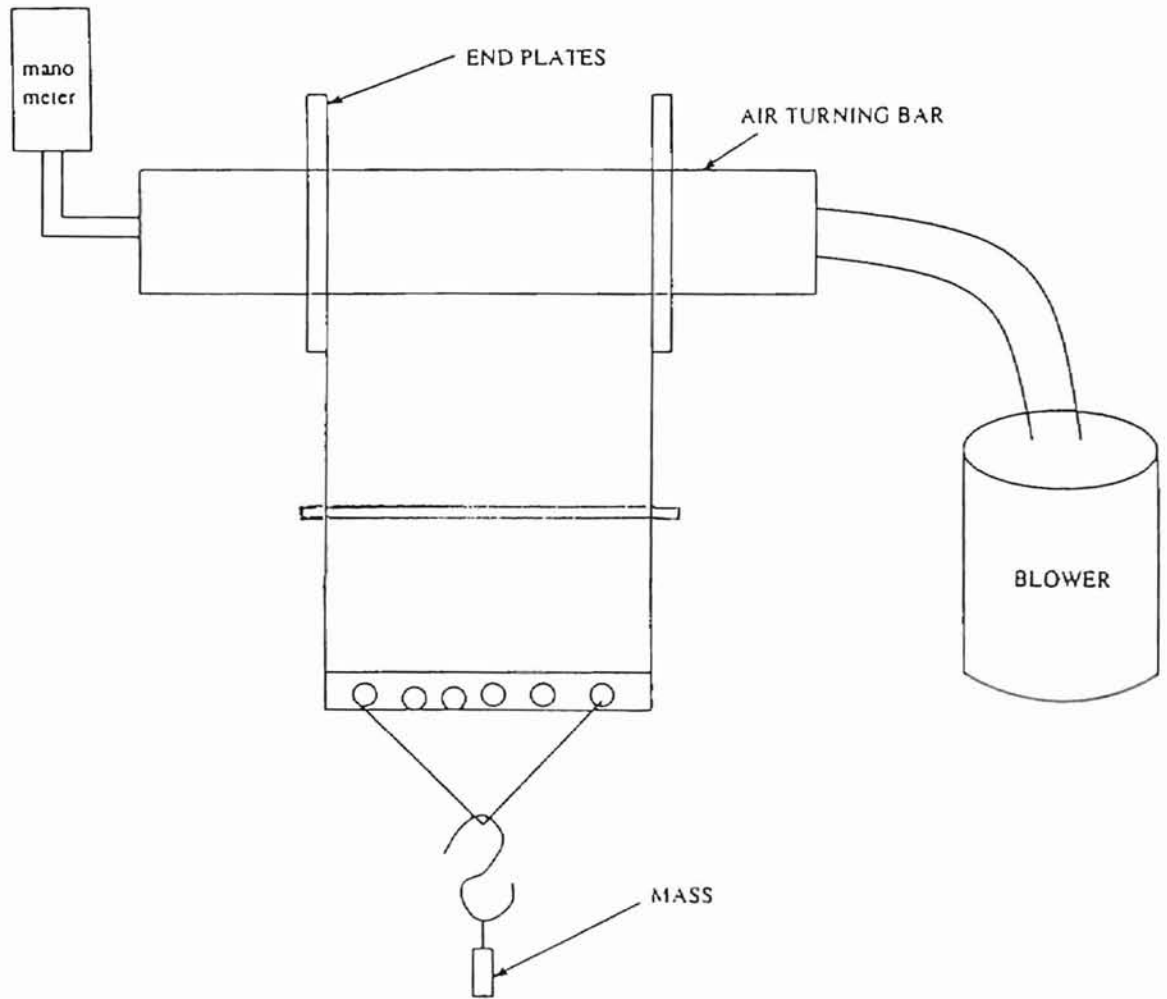


Figure 4.1 Schematic of Web and Air Turning Bar Setup

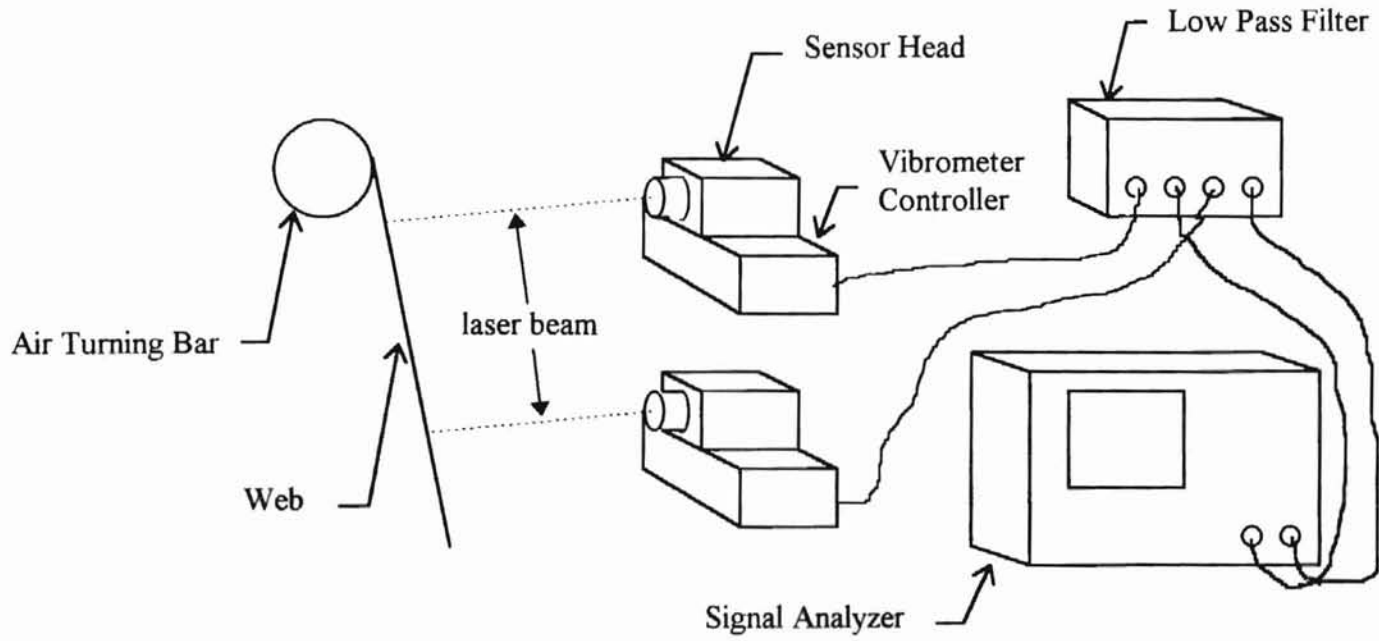


Figure 4.2 Schematic of Measuring Equipment Setup

## 4.2 Results and Discussions

At some operating conditions, the web span between the air turning bar and the adjacent support vibrates at different modes. Usually, the instability was accompanied with a loud noise. This type of instability seems to occur over a wide range of wrap angles. Generally, if there was no air leakage in the operating conditions, the fundamental frequency of flutter was increased with the increase of web tension. There was a narrow range of web tension where large amplitude flutter occurred, and decreasing the web tension did not necessarily cause an increase of flutter amplitudes. Above a certain value of web tension, the flutter was almost non-existent. As the web span was decreased, the flutter frequency was increased. When there was air leakage from the sides of the web, the result became different, as described in the following sections. The fundamental frequency increased when tension increased, as expected; surprisingly it also increased when the span length increased.



#### 4.21 Free-Span Flutter with No Edge Air Leakage

Here, the air leakage from the two edges of the web had small influence, so we assumed that there was no air leakage. It was very obvious that the frequency increased when the tension increased. This always happened regardless of whether the span was short or long. The data shown in Figure 4.3 and Figure 4.4 was tested with the span length 7 inches and the width 6 inches. The test point was 4 inches from the top of the web span, a little lower than the middle of the span. Adjusting the wrap angle until the phenomenon was most obvious, record the wrap angle  $2^\circ$ . The web width was 6 inches, the standard size of test product. Choosing different span lengths, the frequency range was different, but the curves of frequency and amplitude were very similar.

It seems that the frequency increased at both of the ranges of tension (tension per unit width), with the whole range from .083 to 0.2 lb./in. and from 0.25 to 0.41667 lb./in.. The fundamental frequency also increased pretty smoothly. In the range of 0.083 to 0.25 lb./in., usually a second harmonic frequency occurred and sometimes even a third harmonic frequency. The fundamental frequency predominately vibrated. The fundamental frequency controlled the flutter while the tension was at a range of 0.18 lb./in.. During this range, the flutter was relatively simple. Between 0.29 to 0.42 lb./in., the third harmonic frequency vibrated strongest, and the second harmonic frequency was almost non-existent. On the plot, it seems that the leading frequency changed from the fundamental frequency to the third harmonic frequency as the tension increased to 0.29 lb./in.. In the range from 0.083 to 0.33 lb./in., the second harmonic frequency seemed

weak and sometimes disappeared. We can see this in Figure 4.5. Theoretically, we can see that the fundamental frequency increases when tension increases from equation (2.5).

In Figure 4.4, we can see the relationship between  $T/Pd$  (detail in 5.2) and frequency. Since the pressure changed a little in this experiment and the diameter of the air turning bar remained constant, the curve was very similar with the one in Figure 4.3. The fundamental frequency increased very smoothly in the whole range. When  $T/Pd$  ranged from 0.17 to 0.3, the second harmonic frequency was strong sometimes, while the fundamental frequency still led the vibration. In the range from 0.3 to 0.55, the second harmonic frequency almost disappeared and left the fundamental frequency controlling the flutter. In the range of 0.60 to 0.84, the third harmonic frequency came up to lead the flutter and the fundamental frequency was relatively weak. The second harmonic frequency almost disappeared in the range from 0.34 to 0.68, which is exactly the same as the figure for Tension Vs. Frequency.

After testing different spans, we gained very similar results. Regardless of the length of the span, the frequency always increased when the tension increased. The first frequency controlled the vibration until the  $T/Pd$  value was around 0.52, and then the third harmonic frequency took over. The second harmonic frequency was affected more at smaller  $T/Pd$  values than at larger  $T/Pd$  values. Both the first and third frequencies increased smoothly. The second harmonic frequency was unstable in the range of  $T/Pd$  values from 0.18 to 0.68. However, when you change the length of the web, the second harmonic frequency range varies. The tendency for the tension plot was the same for the

T/Pd value of 0.5, when the flutter jumped from first frequency mode to third harmonic frequency mode.

Just as shown in Figure 4.3, one interesting observation was that the frequency increased more while the span was short. With a long span, the curve was smoother. Thus demonstrating that the jumping from first frequency to third harmonic frequency was not as fast. This resulted in a wider range of the second harmonic frequency.

Figure 4.5 showed how amplitude changed when T/Pd increased. The amplitude value read directly from the signal analyzer was voltage. While we chose the function of the average value of some samples, the signal analyzer would automatically give amplitude in root-mean-square voltage, as shown in Table 4.1. The amplitudes were converted to velocity, which were used in the data plot (Figure 4.5), by using equation (4.1). The change of amplitude seems less complex. Using the same operating conditions as the above (span 7 in, wrap angle  $3^\circ$ , test point 4 in. from the top of the web span), we can see that the amplitude was quite large at T/Pd range from 0.2 to 0.5, and that it peaked around T/Pd equals 0.35. As the T/Pd continued to increase, the amplitude did not increase any more. On the contrary, it stayed at lower values. This happened no matter whether the span was short or long. Though the range of T/Pd might not always be from 0.1 to 0.5 where the maximum amplitude appeared, sometimes the range was a little bit bigger or smaller; however, it was usually around T/Pd value of 0.3. Usually, the amplitude of the flutter for T/Pd lower than 0.3 resulted in small waves. In some cases, this part might be a smooth curve.

Wrap angle affects the increasing rate as well. Usually, the smaller the wrap angle, the smoother the curve. However, the difference is not as obvious. During the wrap angle range from  $2^\circ$  to  $12^\circ$ , the frequency results in the maximum amount of amplitude flutter. Within this range, regardless of what the wrap angle was, the whole tendency of the frequency increased along a similar curve. The only difference was in the smoothness of the curve.

One significant result came when there was no air leakage. This was that sometimes it showed that the first frequency led the flutter, but also the second harmonic frequency or even the third harmonic frequency did it at times.

Figure 4.6 is one of the power spectrum plots (raw data in Appendix A). It was tested when the web span was 7 inches, the width was 6 inches, and the wrap angle was  $3.0^\circ$ . This was the source data of Figure 4.3 and Figure 4.4. We can see that the fundamental frequency had the biggest amplitude being much bigger than the second harmonic frequency. This led us to see why the first frequency led the flutter more often than the second or third harmonic frequency. It was possible that the second or even third harmonic frequency affected the web flutter at the same time. Actually, this happened more while the T/Pd was really small. We can read this in Table 4.1. The second harmonic frequency appeared when the T/Pd was 0.08 and 0.17. Increasing T/Pd values caused the third harmonic frequency to lead the flutter. Also this kind of phenomenon happened more often with a short span. With a long web length, only one frequency

appeared. At low  $T/Pd$  values, it was the first frequency; and, at high  $T/Pd$  values it was the third harmonic frequency.

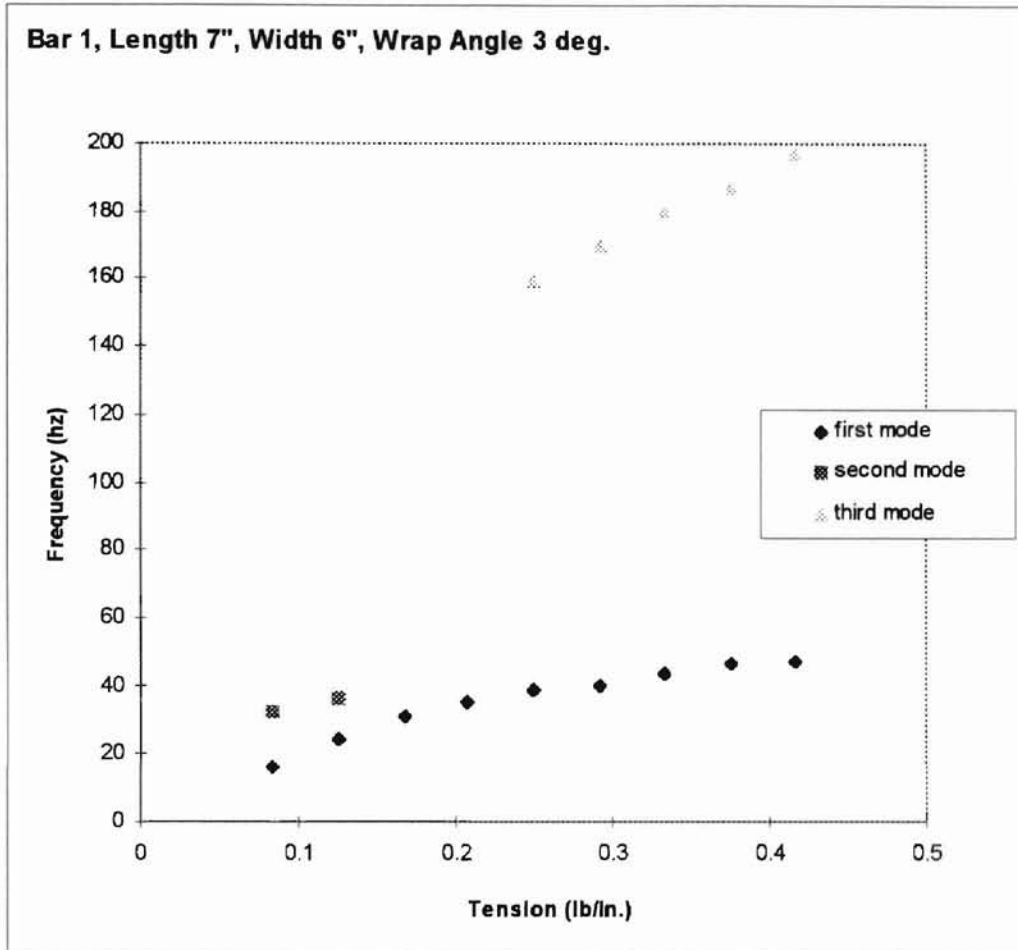


Figure 4.3 Effect of Web Tension on Flutter Frequency

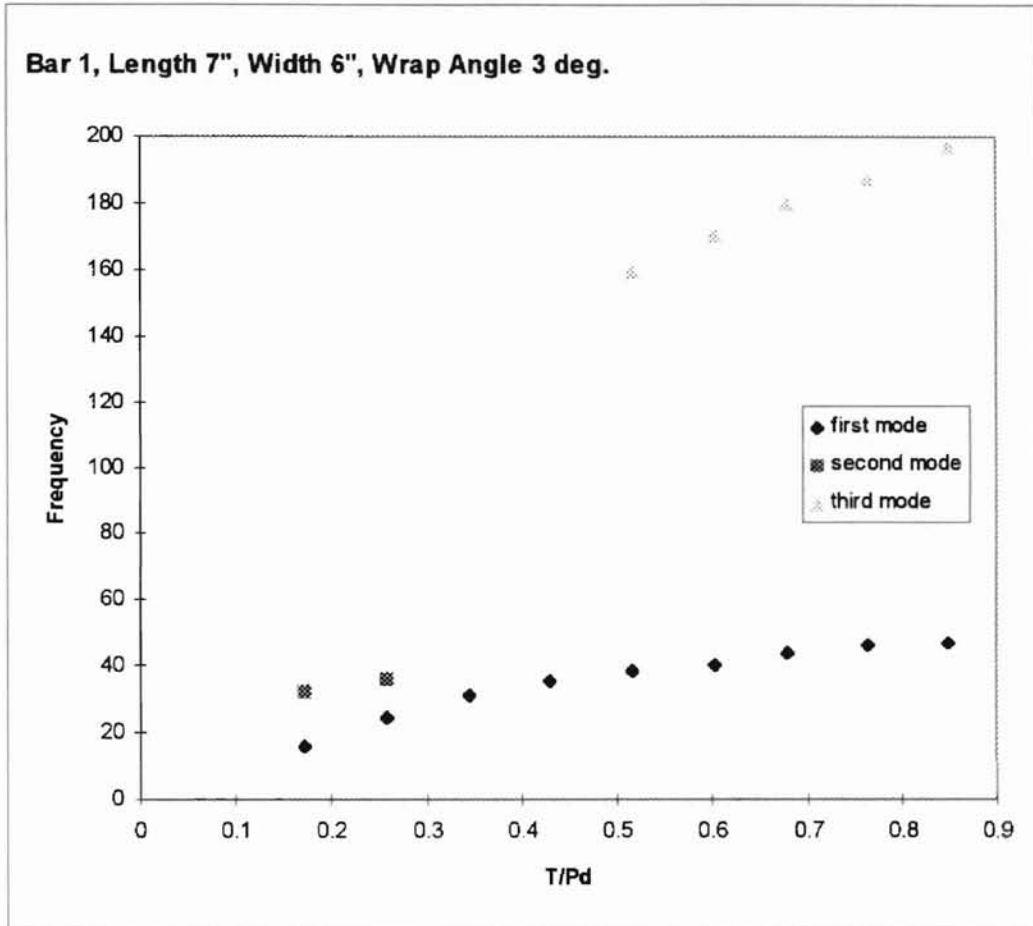


Figure 4.4 Effect of Tension Parameter on Flutter Frequency

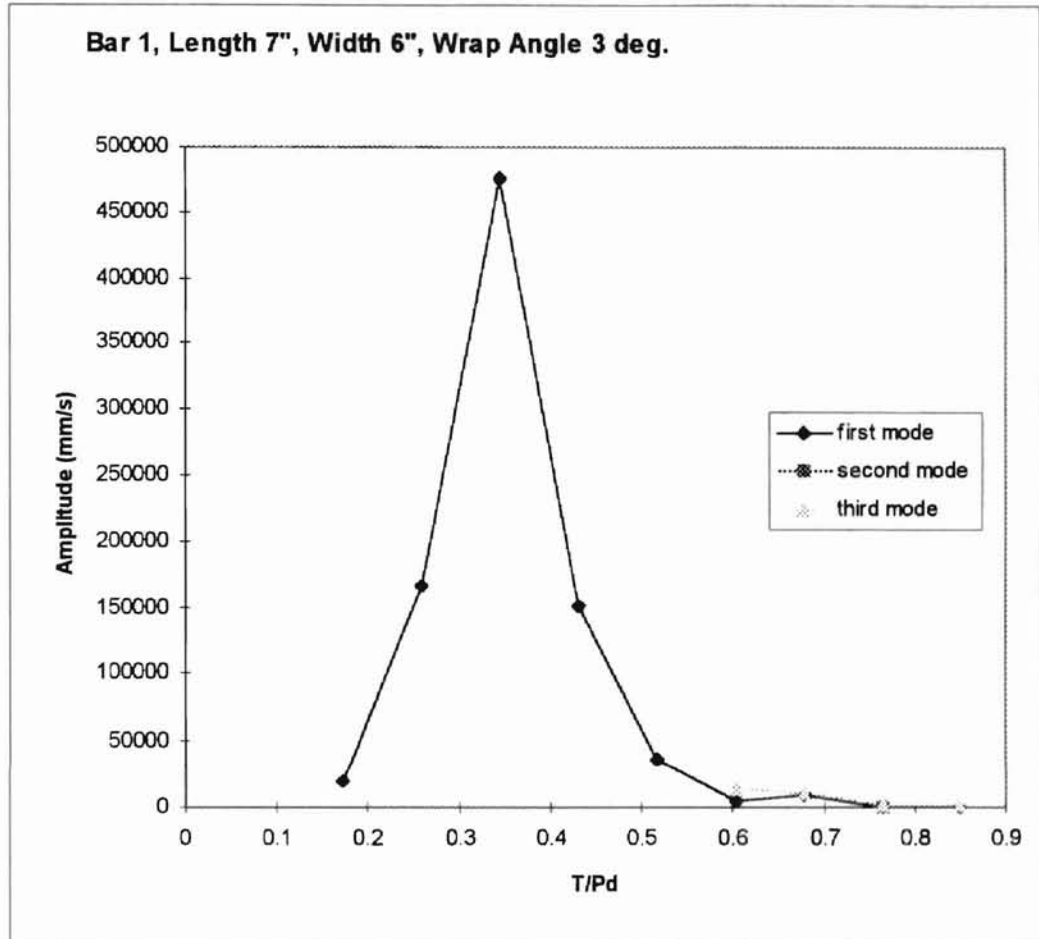


Figure 4.5 Effect of Tension Parameter on Flutter Amplitude



Table 4.1 Data of Frequency and Amplitude (No Air Leakage)

tension (lb.)	L= 7", W=6" pressure (in. water)	$\theta^\circ$	freq. (Hz)	amp (mVrms <sup>2</sup> )
0.50	6.70	3.0	<b>f1=16</b>	1560.00
	6.70		f2=32	
	6.70		f3=47	
0.75	6.70	3.0	<b>f1=24.5</b>	4560.08
	6.70		f2=36	
1.00	6.70	3.0	f=31	7712.70
1.25	6.70	3.0	<b>f1=35</b>	4348.95
	6.70		f2=165	
1.50	6.70	3.0	<b>f1=38.5</b>	2135.90
	6.70		f2=159	
1.75	6.70	3.0	f1=40	780.59
	6.70		<b>f2=170</b>	<b>1334.94</b>
2.00	6.80	3.0	f1=43.5	1040.00
2.25	6.80	1.0	<b>f2=180</b>	<b>1148.51</b>
	6.80		f1=46	142.30
	6.80		f2=116	160.00
2.50	6.80	1.0	<b>f3=187</b>	<b>314.47</b>
	6.80		f1=47	141.90
	6.80		<b>f2=121</b>	<b>324.68</b>
			f3=197	

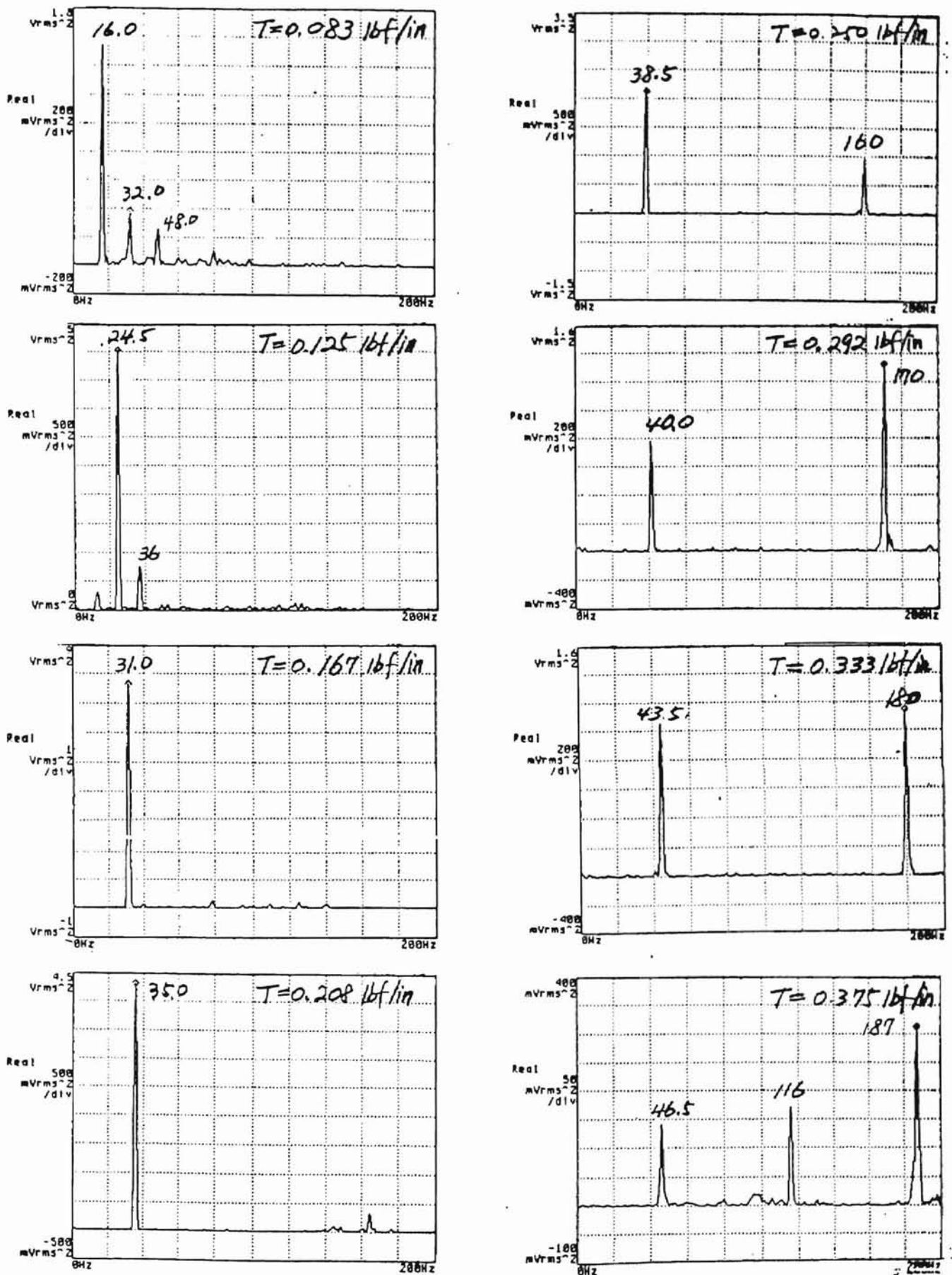


Figure 4.5 Spectrum Plot (no Air Leakage)

#### 4.22 Free-Span Flutter with Edge Air Leakage

Because of the situation of the set up, it was hard to avoid the air leakage from the two edges of the web. In most cases, there was always some air leakage. Actually, we found an interesting phenomenon under the situation with edge air leakage. The most obvious phenomenon resulting from no air leakage was that the fundamental frequency was very strong. This caused the second and third frequencies to be insignificant. We will discuss this in further detail in the following parts of this section.

## Effect of Edge Gap

Considering the accuracy of the experiment, some tests were done to see the effects on the edge gap size on the air leakage. We found some significant differences in the flutter as a result of the gaps with and without air leakage.

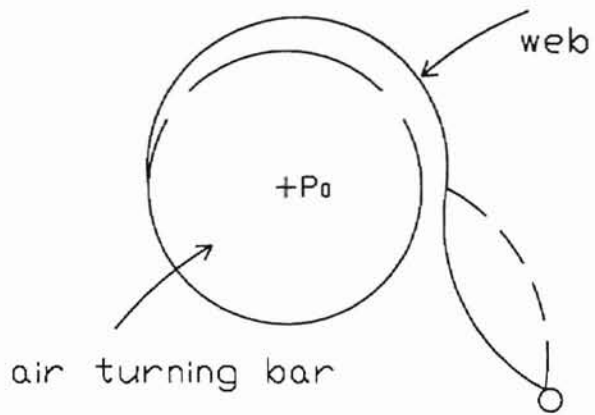
It was found that when the gap was greater than 0.1 in. (1.67% of web width), there would be no change of frequency and vibration modes. This occurred when the gap was on either one side or both sides of the web. Regardless of whether or not the gap increased, the frequency and flutter mode remained quite stable. But, when the gap was less than 1.67% of the web width, the mode became unstable and the frequency was different. When the gap was less than 0.05 in. (0.832% of the web length), the phenomenon was very similar to that of no air leakage.

The gap leakage effect was tested with a span of 9.5 inches long and 6 inches wide. It was found the phenomenon happened in widest tension range at this span length, compared to the other lengths. When the gap was 0.1 in. (1.67% of web length), it buzzed at small tensions (tension per unit width) which were equal to or less than 0.125 lb./in.. When the tension was greater than 0.167 lb./in., it stabilized at 3 nodes mode (see Table 4.2). Different wrap angles were tested, and it appeared to not affect the stability of the flutter. The pictures of different modes are shown in Figure 4.7.

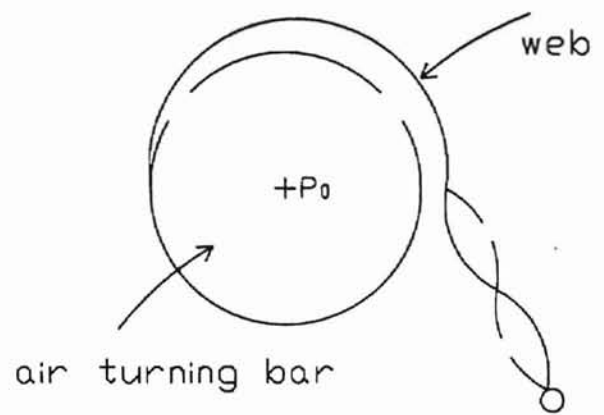
Table 4.2 Effect of Wrap Angle with Big Gap

T/Pd	pressure (in. water)	$\theta^\circ$	f1 (Hz)	f2 (Hz)	f3 (Hz)	shape
0.125	6.75	5.0	21	50.5	128	buzz
0.125	6.8	1.0	18.5	60		buzz
0.167	6.95	1.0	53	106	158	3 nodes
0.167	6.85	4.0	52	104	156	3 nodes
0.208	7	5.0	60.5	120		3 nodes

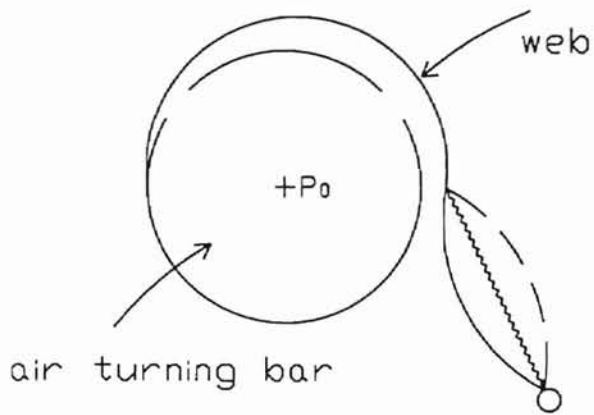
With the same operating conditions as above, it seemed that wrap angle was quite an influential factor when tested with smaller gap 0.05 in. (0.083% of web width). Changing the wrap angle could cause different modes. Thus, it is similar to Table 4.1, because, it virtually impossible to have no air leakage in our experiment.



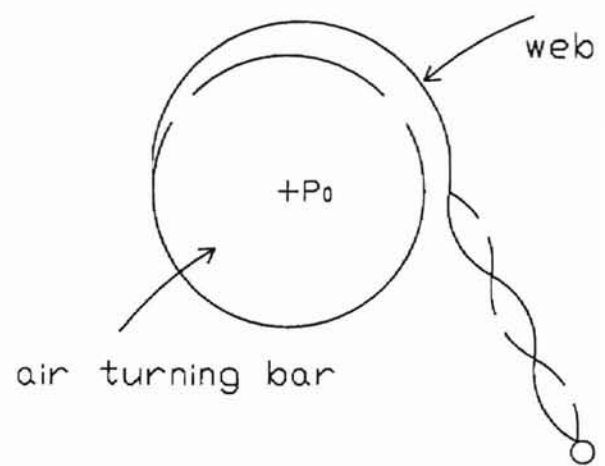
(a) 2 nodes



(b) 3 nodes



(c) 2 nodes & buzz mix



(d) 4 nodes

Figure 4.7 Different Modes

## Wrap Angle

The wrap angle  $\theta$  ( $\alpha$ - $\beta$ ) is an important factor for the different modes while the gap is about 0.083% of the web width (see Table 4.3). It was tested with 9.5 inches long span and 6 inches wide web. When the pressure was 6.95 inches of and tension was 0.125 lb./in., it showed 3 nodes type at 2.0° wrap angle. With the same operating conditions, it showed 2 & 3 nodes mixed at an 0° angle. When the pressure was 7.15 inches of water and the tension was 0.167 lb./in., the vibration was 3 nodes at an 4° angle. However, buzzing & 2 nodes mixed occurred at an 0° angle. Also, in the case where the pressure was 6.95 inches of water and the tension was 0.167 lb./in., it showed 3 nodes vibration at an 3.0° angle and 2 nodes at an 1.0° angle. When an increase in tension occurred after the tension was 0.25 lb./in., the 3 nodes flutter was very stable and there was no fluctuation of flotation height. The accuracy of the wrap angle reading was 0.5°.

The wrap angle was so sensitive that the test result of the wrap angle was not repeatable unless the test conditions were exactly the same. Any little change of the operation condition will cause the result different. In this test, the wrap angle and the tension were changed at the same time; therefore, it is hard to determine the exact effect of the wrap angle. There is some effect, however, this must be determined by further experiments.

Table 4.3 Wrap Angles with Different Modes

tension (lb./in.)	pressure (in. water)	angle (deg.)	mode
0.125	7.00	0.0	2 & 3 nodes mixed
0.125	7.00	2.0	3 nodes
0.125	6.85	6.0	bumping
0.167	7.15	4.0	3 nodes
0.167	7.15	0.0	buzzing & 2 nodes mixed
0.167	6.95	1.0	2 nodes
0.167	6.95	3.0	3 nodes
0.250	7.00	6.0	3 nodes

Test web was 9.5 in. span length and 6 in. width.



## Effect of Tension

It seems that there is a large air leakage effect on small tension. For example, if the tension is at 0.125 lb./in. and the gap on both sides is 0.083% of the web width at the beginning, the phenomenon is very complex. Several modes appear at the same time. When keeping the left side gap fixed and increasing the right side, the phenomenon became more stable until it became a three-node mode. The opposite occurred when the left side gap was fixed and the right side was decreased. The closer the plate got to the web edge, the more unstable the flutter became. Finally when the gap was back to 0.083% of the web width, the web buzzed.

The same test was tried with the tension fixed at 0.25 lb./in. When increasing or decreasing the gap, the frequency didn't change much and the phenomenon remained stable.

One interesting point is that the phenomenon remained the same regardless of whether one side edge reached a certain value or both side edges reached the value. Thus we may say that it did not depend on how much the total gap value was, but what the largest gap value was.

Also, the frequency increases when the tension increases. It happens when there is air leakage and no air leakage. This can be explained with equation (2.5) in chapter 2, that the fundamental frequency increases when tension increases. We can see it in Figure 4.11.

### Effect of Tension Parameter T/Pd

The frequency increased smoothly when the T/Pd increased. This smoothness occurred when the gap value was greater than or equal to 1.67%. This test was done with the web length of 9.5 inches. The frequency change differed compared to no air leakage, which we discussed in section 1 of this chapter. Here, only one frequency predominately led the flutter.

The amplitude changed a lot In the range of T/Pd from 3 to 3.4 and peaked at 3.2. While T/Pd was smaller than 3 or bigger than 3.5, the amplitude was small and didn't change much. With continual increasing T/Pd, the amplitude value remained small until the flutter phenomenon was invisible. Simply, the amplitude did not necessarily increase when T/Pd decreased (shown in Figure 4.8).

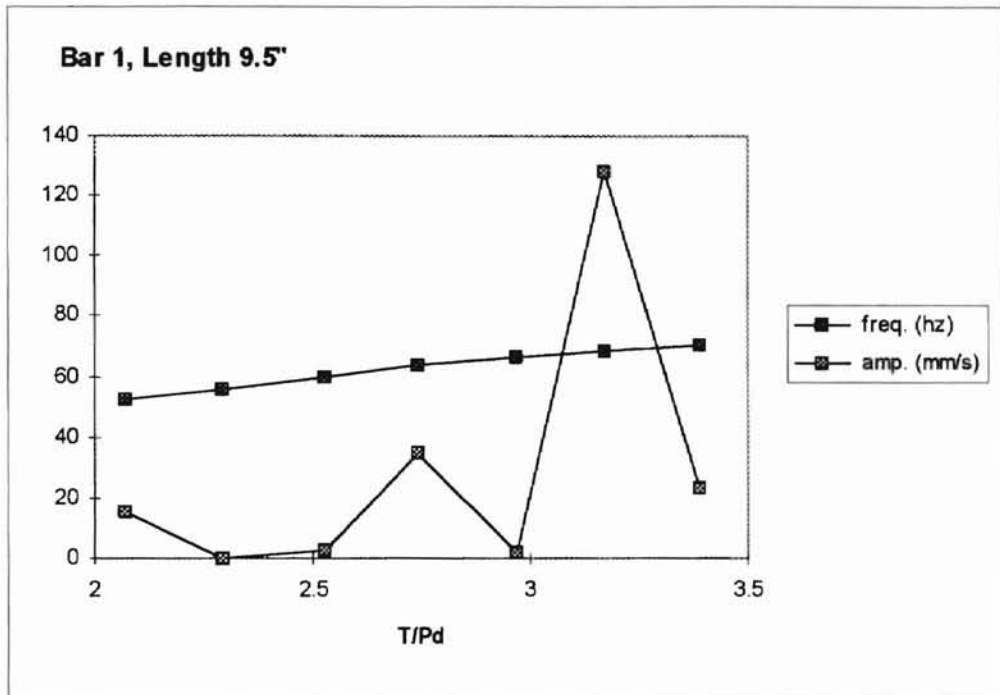


Figure 4.8 Effect of Tension Parameter on Flutter Amplitude and Frequency

## Effect of Pressure

The effect of pressure was tested when the tension was constant at 0.2 lb./in., and the length was 9.5 inches, test point was 4 inches from the top of the web span. From Figure 4.9, we can see that in the same operating conditions, the frequency was not affected much by pressure. Changing the pressure from 0.16 to 0.24 psi, (actually from 4.55 to 6.6 inches of water), the frequency was about 53 Hz changing only 1.5 Hz. Every data in the plot was the average of 30 samples. The phenomenon was stable at 3 nodes mode. We may assume that the air excitation favors at certain frequencies.

The uncertainty of the pressure reading was 0.05 inch water. The pressure was changed by reducing the air flow into the vacuum. The pressure range was from 4.55 to 6.6 inches of water.

The amplitude seems to be affected more than the frequency. With the same pressure change, the amplitude changed from 0 to 3.6 mm/s while the pressure changed from 0.182 to 0.2 psi. The amplitude tended to be maximum at pressure around 0.2 psi. As we mentioned before, the absolute amplitude value was not reproducible. The frequency value and the amplitude trends were the same at different test locations. When the pressure was less than 0.18 psi, the amplitude was almost zero. When the pressure was larger than 0.2 psi, continuous increases in the pressure didn't cause increasing in the amplitude. This is shown in Figure 4.10.

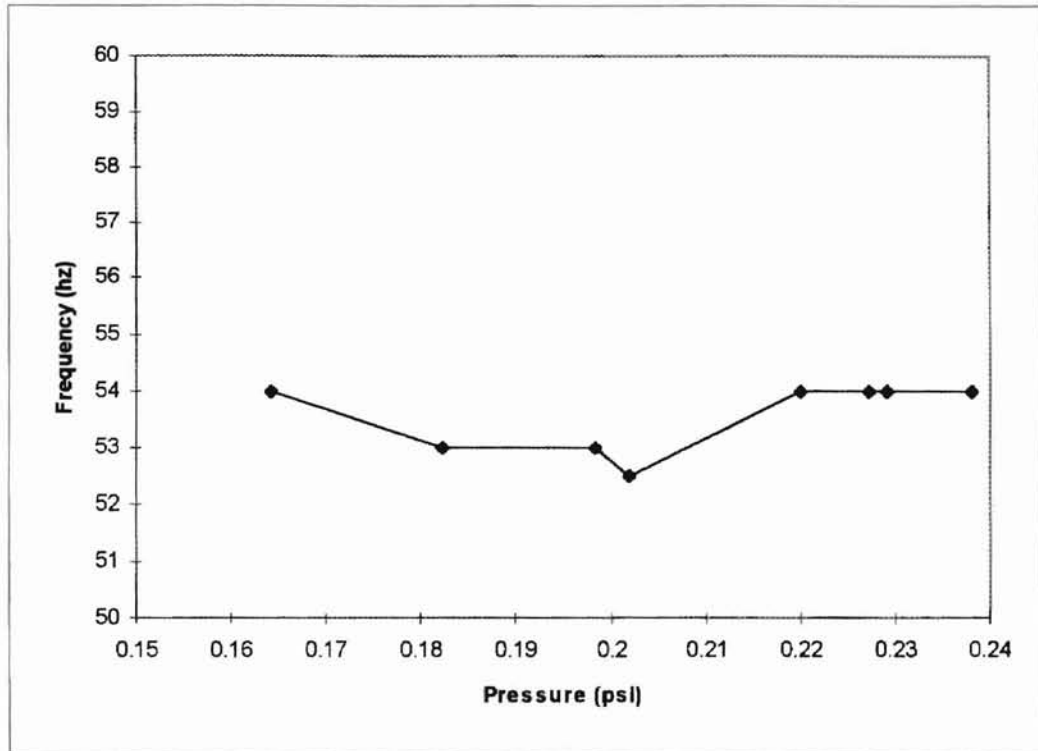


Figure 4.9 Effect of Pressure on Flutter Frequency

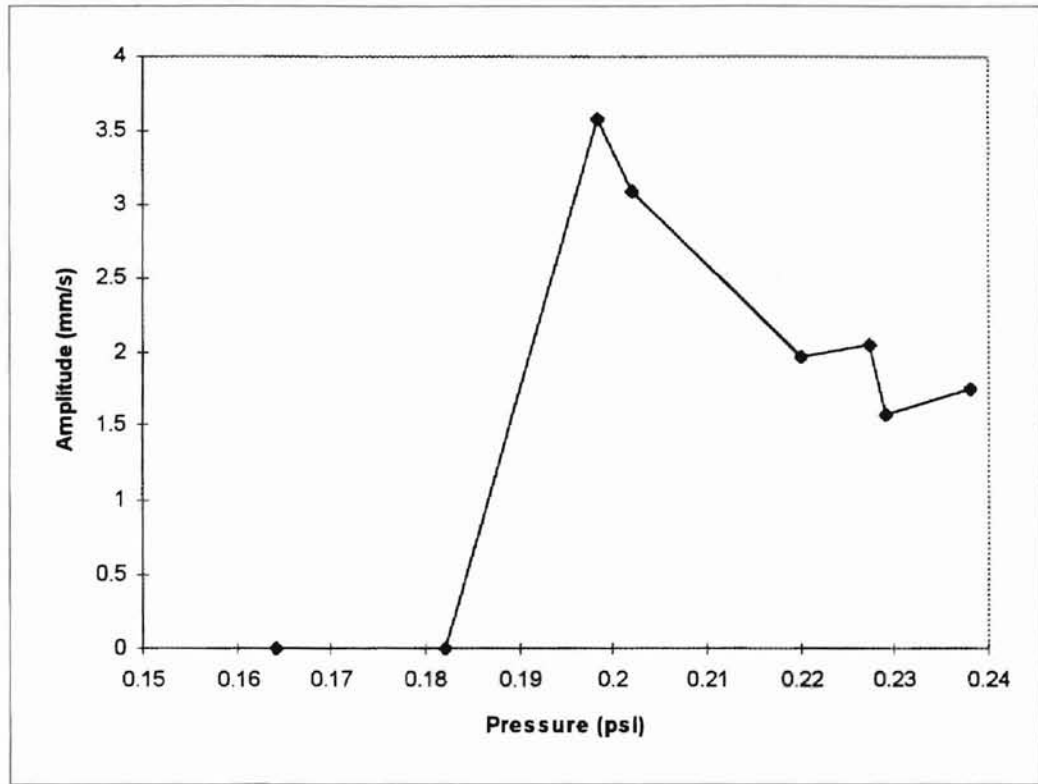


Figure 4.10 Effect of Pressure on Flutter Amplitude

## Effect of Length

Generally, we believe that the frequency increases when length decreases, like shown in equation (2.5). Unexpectedly, the frequency increased when the length increased, jumping to higher modes. From Figure 4.11, we can see this very clearly. With the same tension less than 0.229 lb./in., we see that the longer the length, the larger the frequency in four cases. When the tension was greater than 0.25 lb./in., only the shortest length (5.5 in.) showed the fundamental frequency jumping to the third harmonic frequency for higher tensions. The other three lengths showed no difference at small tension. It appears that the flutter was more unstable at a shorter spans.

It was also found that when the length increased, the number of nodes increased. In our experiments, when the length was 5.5 in. or 7 in., it could be 2 or 3 nodes mode. The 2 nodes mode happened in bigger ranges of wrap angle at length 5.5 in. When the length was 9.5 in., it was just 3 nodes mode. When the length became 11 in., it showed 4 nodes mode. Longer lengths were tested. Since the amplitude was very small, it was hard to tell how many nodes were there.

Now we use non-dimensional parameter  $L/d$  ( $L$  is length of web span,  $d$  is diameter of air turning bar, detail of  $L/d$  is discussed in section 5.2) to analyze the phenomenon. In Figure 4.12, we can see that the frequency increases when  $L/d$  increases under different tension per unit width. The increasing rate curve was very smooth.

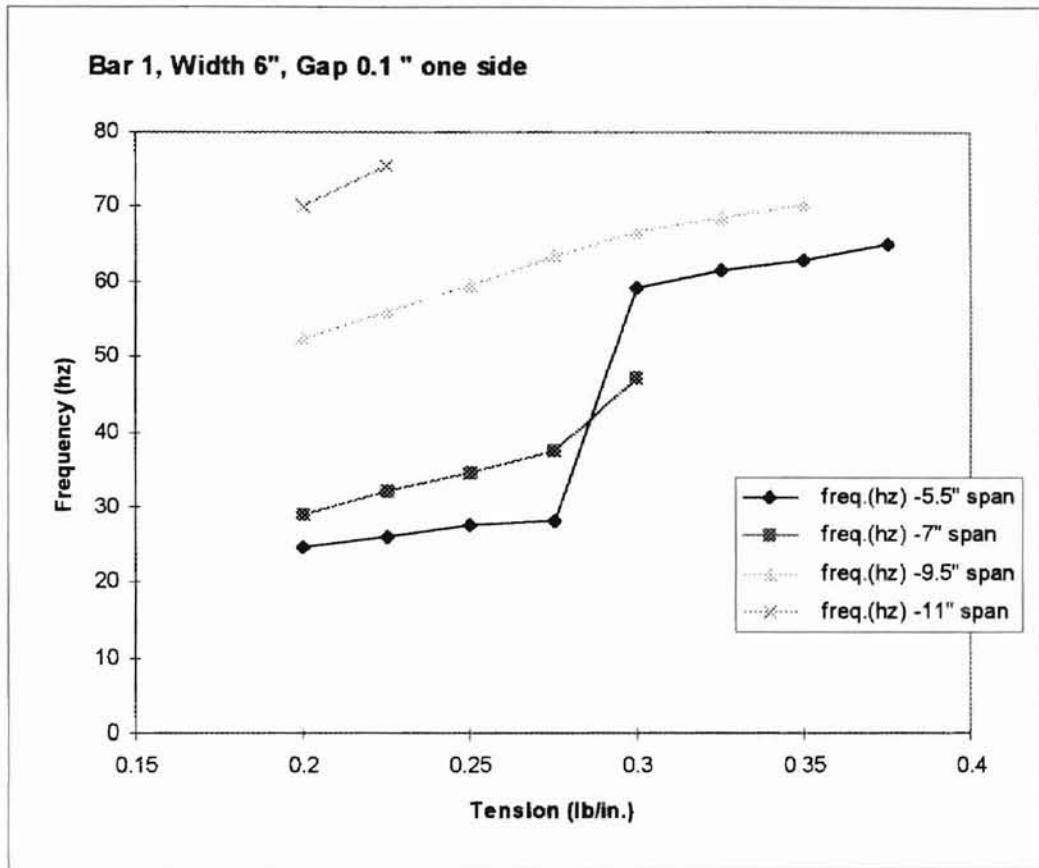


Figure 4.11 Effect of Web Tension and Length on Flutter Frequency



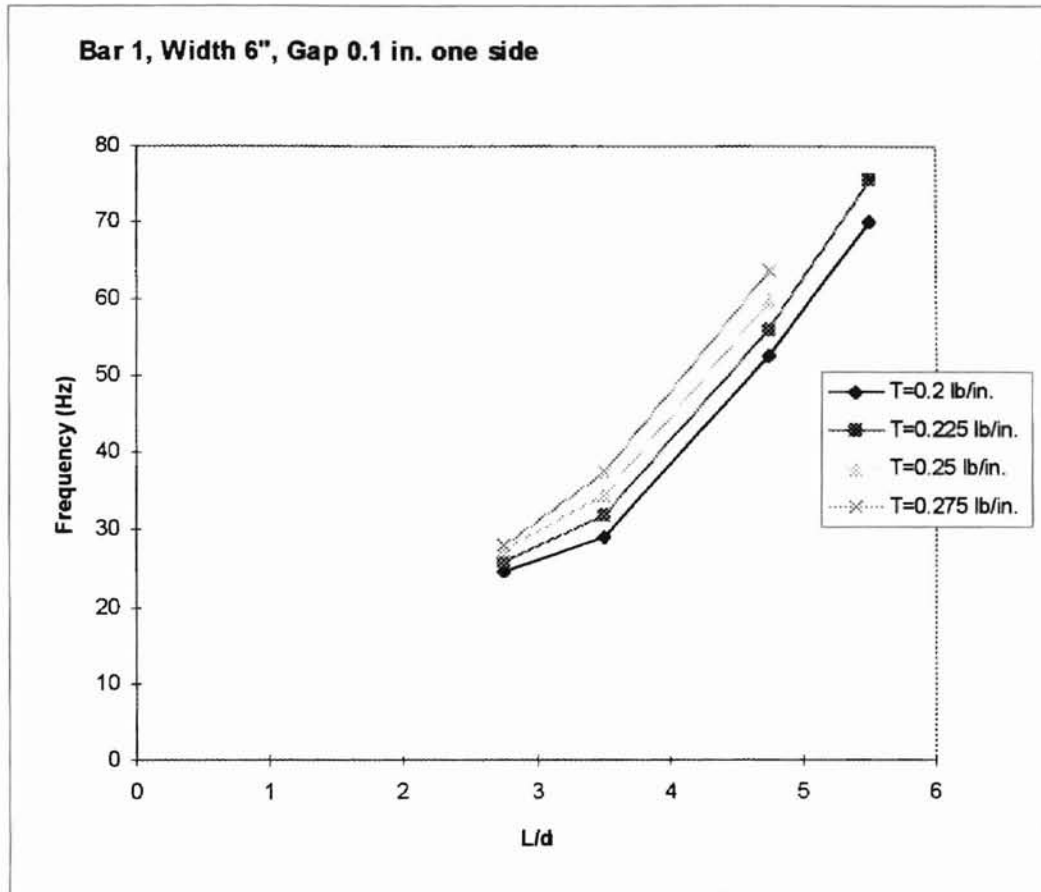


Figure 4.12 Effect of Length Parameter on Flutter Frequency

## Phase Shift

Though there were several different flutter modes, as shown in Figure 4.7, they all seem like traveling wave. It was expected that there would be phase shift during the wave traveling. Since the web vibrated most in the three-node mode, this case was chosen to measure the phase shift along the web span. The test used a 9.5 inches length span. The first vibrometer measurement location was 4 inches from the top of the web span, and it was fixed. The second test point was moved away from the first one, until the distance between these two locations increased to 0.5 span.

In Figure 4.13, we can see that when the distance between the two test points was almost half a span, the phase shift was nearly  $180^\circ$  (consider  $-50^\circ$  at distance of 0,  $158^\circ$  at distance of 0.5 span).

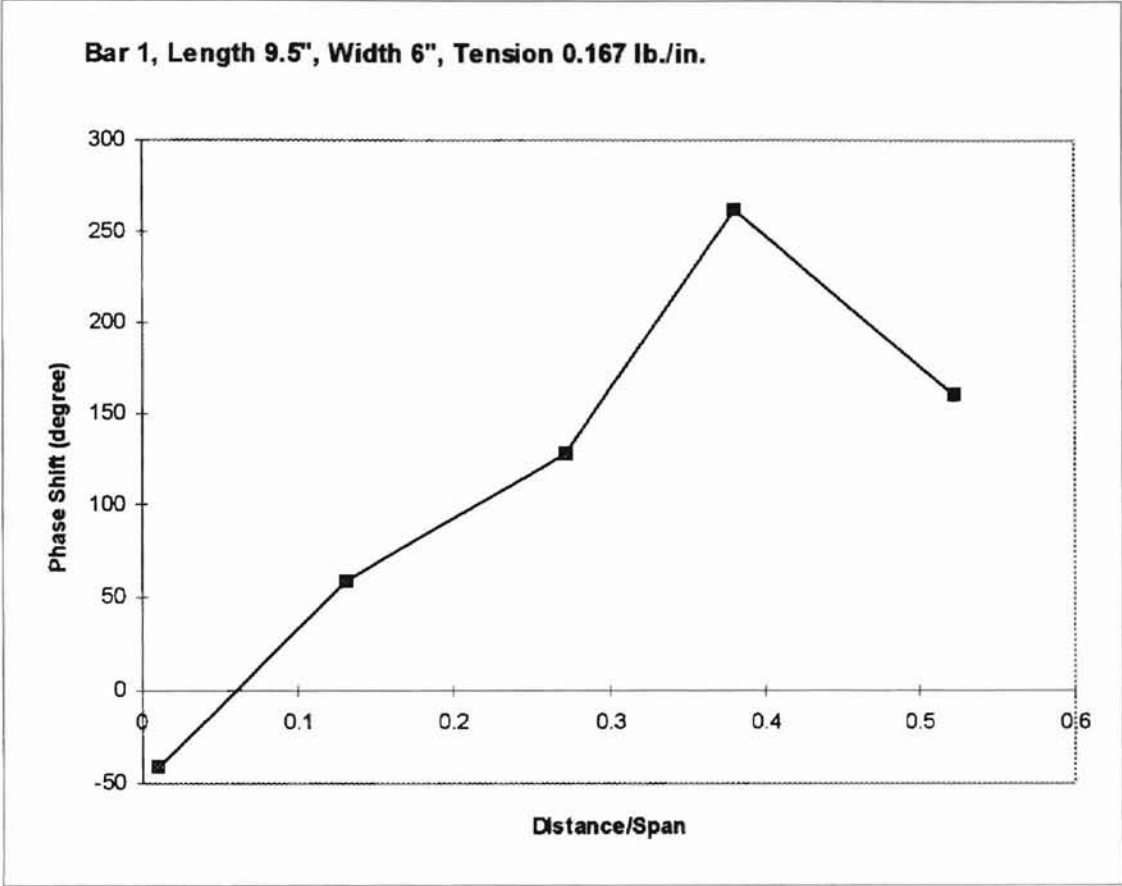


Figure 4.13 Phase Shift

## CHAPTER V

### NONDIMENSIONAL PARAMETERS

#### 5.1 Introduction of $\pi$ Theorem

Since the existing critical condition equations (equation (2.1),(2.2),(2.3) and (2.4)) could not successfully explain our test result, nondimensional parameters were used to try to do some nondimensional analysis. Dimensional analysis is a method for reducing the number and complexity of experimental variables which affect a given physical phenomenon, using a sort of compacting technique. If a phenomenon depends upon  $n$  dimensional variables, dimensional analysis will reduce the problem to only  $k$  dimensionless variables, where the reduction  $j = n - k = 1, 2, 3$ , or 4, depending upon the problem complexity. Usually the reduction  $n - k$  equals the number of different fundamental dimensions which govern the problem.

There are several methods of reducing a number of dimensional variables into a smaller number of dimensionless groups. One of the most popular ones is *Buckingham pi theorem*.  $\pi$  means a product of variables. If a physical process involves  $n$  dimensional variables, it can be reduced to a relation between only  $k$  dimensionless variables or  $\pi$ 's. The reduction  $j = n - k$  equals the maximum number of variables which do not form a  $\pi$  among themselves and is always less than or equal to the number of dimensions describing the variables. Find  $j$ , then select  $j$  variables which do not form a  $\pi$  among themselves.

## 5.2 Nondimensional Parameters

There are 3 fundamental dimensions ( $MLT$ ): mass  $M$ , length  $L$ , and time  $T$  are involved in the analysis of the experiment. That is  $j = 3$ . There are 10 independent variables and 2 dependent variables, so  $n = 10 + 2 = 12$ . Thus  $n - j = 12 - 3 = 9 = k$ .

Step 1. List and count the dimensions of each variable (refer to Table 5.1).

Step 2. Select a set of fundamental dimensions:  $M, L, T$ .

Step 3. Select repeating parameters:  $T, \gamma, d$ .

Step 4. Set up dimensional equations combining the parameters selected in last step with each of the other parameters.

So there should be  $12 - 3 = 9 \pi$ 's, for  $\alpha$  doesn't have dimension, so there will be 11  $\pi$ 's.

Table 5.1 List of Variables and Dimensions

	<b>Dependent Variable</b>	<b>Symbol</b>	<b>Dimensions</b>
1	Frequency	f	$T^{-1}$
2	Flow Velocity	U	$LT^{-1}$
3	Amplitude	a	L
4	Tension Per Unit Width	T	$MT^{-2}$
5	Mass Per Unit Width	m	$ML^{-1}$
6	Wrap Angle	$\theta$	
7	Stiffness of Web Per Unit Width	D	$ML^2T^{-2}$
8	Pressure	P	$ML^{-1}T^{-2}$
9	Diameter of The Air Bar	d	L
10	Web Length	L	L
11	Mass Density of The Web	$\gamma$	$ML^{-2}$
12	Volume Flow Rate Per Unit Width	Q	$L^2T^{-1}$
13	Air Density	$\rho$	$ML^{-3}$
14	Kinematic Viscosity	$\nu$	$L^2T^{-1}$
15	Wavelength	$\lambda$	L

Step 4, searching  $\pi$ 's.

**Case 1:**

$$\begin{aligned}\pi_1 &= (T^a \cdot \gamma^b \cdot d^c) m^d \\ &= (MT^2)^a \cdot (ML^{-2})^b \cdot (L)^c \cdot (ML^{-1})^d \\ &= M^{(a+b+d)} \cdot L^{(-2b+c-d)} \cdot T^{(-2a)} \\ &= M^0 \cdot L^0 d T^0\end{aligned}$$

$$\begin{aligned}\text{where} \quad a + b + d &= 0 \\ -2b + c - d &= 0 \\ -2a &= 0\end{aligned}$$

By solving the above simultaneous equations, we have:

$$\begin{aligned}a &= 0 \\ b &= -d \\ c &= b\end{aligned}$$

Let  $b = 1$ , so

$$\begin{aligned}a &= 0 \\ b &= 1 \\ c &= 1 \\ d &= -1\end{aligned}$$

Therefore,  $\pi_1 = (\gamma d) / m$

**Case 2:**

$$\begin{aligned}\pi_2 &= (T^a \cdot \gamma^b \cdot d^c) D^d \\ &= (MT^2)^a \cdot (ML^{-2})^b \cdot (L)^c \cdot (ML^2T^2)^d \\ &= M^{(a+b+d)} \cdot L^{(-2b+c+2d)} \cdot T^{(-2a-2d)} \\ &= M^0 \cdot L^0 \cdot d T^0\end{aligned}$$

where

$$\begin{aligned}a + b + d &= 0 \\ -2b + c + 2d &= 0 \\ -2a - 2d &= 0\end{aligned}$$

By solving the above simultaneous equations, we have:

$$\begin{aligned}a &= -d \\ b &= 0 \\ c &= -2d\end{aligned}$$

Let  $a = 1$ , so

$$\begin{aligned}a &= 1 \\ b &= 0 \\ c &= 2 \\ d &= -1\end{aligned}$$

Therefore,  $\pi_2 = (Td^2) / D$

**Case 3:**

$$\begin{aligned}\pi_3 &= (T^a \cdot \gamma^b \cdot d^c) P^d \\ &= (MT^2)^a \cdot (ML^{-2})^b \cdot (L)^c \cdot (ML^{-1}T^2)^d \\ &= M^{(a+b+d)} \cdot L^{(-2b+c-d)} \cdot T^{(-2a-2d)} \\ &= M^0 \cdot L^0 \cdot T^0\end{aligned}$$



where

$$\begin{aligned}
 a + b + d &= 0 \\
 -2b + c - d &= 0 \\
 -2a - 2d &= 0
 \end{aligned}$$

By solving the above simultaneous equations, we have:

$$\begin{aligned}
 a &= -d \\
 b &= 0 \\
 c &= d
 \end{aligned}$$

Let  $a = 1$ , so

$$\begin{aligned}
 a &= 1 \\
 b &= 0 \\
 c &= -1 \\
 d &= -1
 \end{aligned}$$

Therefore,  $\pi_3 = T/(Pd)$

**Case 4:**

$$\begin{aligned}
 \pi_4 &= (T^a \cdot \gamma^b \cdot d^c) L^d \\
 &= (MT^2)^a \cdot (ML^{-2})^b \cdot (L)^c \cdot (L)^d \\
 &= M^{(a+b)} \cdot L^{(-2b+c+d)} \cdot T^{(-2a)} \\
 &= M^0 \cdot L^0 \cdot T^0
 \end{aligned}$$

where

$$\begin{aligned}
 a + b &= 0 \\
 -2b + c + d &= 0 \\
 -2a &= 0
 \end{aligned}$$

By solving the above simultaneous equations, we have:

$$\begin{aligned}a &= 0 \\b &= 0 \\c &= -d\end{aligned}$$

Let  $c = 1$ , so

$$\begin{aligned}a &= 0 \\b &= 0 \\c &= 1 \\d &= -1\end{aligned}$$

Therefore,  $\pi_4 = d/L$

Case 5:

$$\begin{aligned}\pi_5 &= (T^a \cdot \gamma^b \cdot \mathcal{F}^c) Q^d \\&= (MT^2)^a \cdot (ML^{-2})^b \cdot (L)^c \cdot (L^2 T^1)^d \\&= M^{(a+b)} \cdot L^{(-2b+c+2d)} \cdot T^{(-2a-d)} \\&= M^0 \cdot L^0 \cdot T^0\end{aligned}$$

where

$$\begin{aligned}a + b &= 0 \\-2b + c + 2d &= 0 \\-2a - d &= 0\end{aligned}$$

By solving the above simultaneous equations, we have:

$$\begin{aligned}a &= -b \\c &= 2a \\d &= -2a\end{aligned}$$

Let  $a = 1$ , so

$$a = 1$$

$$b = -1$$

$$c = 2$$

$$d = -2$$

Therefore,  $\pi_5 = (Td^2) / (\gamma Q^2)$

**Case 6:**

$$\begin{aligned}\pi_6 &= (T^a \cdot \gamma^b \cdot d^c) \rho^d \\ &= (MT^2)^a \cdot (ML^{-2})^b \cdot (L)^c \cdot (ML^{-3})^d \\ &= M^{(a+b+d)} \cdot L^{(-2b+c-3d)} \cdot T^{(-2a)} \\ &= M^0 \cdot L^0 \cdot T^0\end{aligned}$$

where

$$\begin{aligned}a + b + d &= 0 \\ -2b + c - 3d &= 0 \\ -2a &= 0\end{aligned}$$

By solving the above simultaneous equations, we have:

$$a = 0$$

$$b = -d$$

$$c = d$$

Let  $d = 1$ , so

$$a = 0$$

$$b = -1$$

$$c = 1$$

$$d = 1$$

Therefore,  $\pi_6 = (\rho d) / \gamma$

**Case 7:**

$$\begin{aligned}\pi_7 &= (T^a \cdot \gamma^b \cdot d^c) v^d \\ &= (MT^2)^a \cdot (ML^{-2})^b \cdot (L)^c \cdot (L^{-1}T^1)^d \\ &= M^{(a+b)} \cdot L^{(-2b+c+2d)} \cdot T^{(-2a-d)} \\ &= M^0 \cdot L^0 \cdot T^0\end{aligned}$$

where

$$\begin{aligned}a + b &= 0 \\ -2b + c + 2d &= 0 \\ -2a - d &= 0\end{aligned}$$

By solving the above simultaneous equations, we have:

$$\begin{aligned}a &= -b \\ d &= -2a \\ c &= -d\end{aligned}$$

Let  $a = 1$ , so

$$\begin{aligned}a &= 1 \\ b &= -1 \\ c &= 2 \\ d &= -2\end{aligned}$$

Therefore,  $\pi_7 = (Td^2) / (\gamma v^2)$

**Case 8:**

$$\begin{aligned}
\pi_8 &= (T^a \cdot \gamma^b \cdot d^c) \lambda^d \\
&= (MT^2)^a \cdot (ML^{-2})^b \cdot (L)^c \cdot (L)^d \\
&= M^{(a+b)} \cdot L^{(-2b+c+d)} \cdot T^{(-2a)} \\
&= M^0 \cdot L^0 \cdot T^0
\end{aligned}$$

where

$$\begin{aligned}
a + b &= 0 \\
-2b + c + d &= 0 \\
-2a &= 0
\end{aligned}$$

By solving the above simultaneous equations, we have:

$$\begin{aligned}
a &= 0 \\
b &= 0 \\
c &= -d
\end{aligned}$$

Let  $c = 1$ , so

$$\begin{aligned}
a &= 0 \\
b &= 0 \\
c &= 1 \\
d &= -1
\end{aligned}$$

Therefore,  $\pi_8 = d / \lambda$

**Case 9:**

$$\begin{aligned}
\pi_9 &= (T^a \cdot \gamma^b \cdot d^c) U^d \\
&= (MT^2)^a \cdot (ML^{-2})^b \cdot (L)^c \cdot (LT^1)^d \\
&= M^{(a+b)} \cdot L^{(-2b+c+d)} \cdot T^{(-2a+d)} \\
&= M^0 \cdot L^0 \cdot T^0
\end{aligned}$$

where

$$\begin{aligned} a + b &= 0 \\ -2b + c + d &= 0 \\ -2a - d &= 0 \end{aligned}$$

By solving the above simultaneous equations, we have:

$$\begin{aligned} a &= -b \\ d &= -2a \\ c &= 0 \end{aligned}$$

Let  $b = 1$ , so

$$\begin{aligned} a &= -1 \\ b &= 1 \\ c &= 0 \\ d &= 2 \end{aligned}$$

Therefore,  $\pi_9 = (\gamma U^2) / T$

**Case 10:**

$$\begin{aligned} \pi_{10} &= (T^a \cdot \gamma^b \cdot c^c) f^d \\ &= (MT^2)^a \cdot (ML^{-2})^b \cdot (L)^c \cdot (T^{-1})^d \\ &= M^{(a+b)} \cdot L^{(-2b+c)} \cdot T^{(-2a-d)} \\ &= M^0 \cdot L^0 \cdot T^0 \end{aligned}$$

where

$$\begin{aligned} a + b &= 0 \\ -2b + c &= 0 \\ -2a - d &= 0 \end{aligned}$$

By solving the above simultaneous equations, we have:

$$a = -b$$

$$d = -2a$$

$$c = 2b$$

Let  $b = 1$ , so

$$a = -1$$

$$b = 1$$

$$c = 2$$

$$d = 2$$

Therefore,  $\pi_{10} = (\gamma d^2 f^2) / T$

#### Case 11:

$$\begin{aligned}\pi_4 &= (T^a \cdot \gamma^b \cdot d^c) a^d \\ &= (MT^2)^a \cdot (ML^{-2})^b \cdot (L)^c \cdot (L)^d \\ &= M^{(a+b)} \cdot L^{(-2b+c+d)} \cdot T^{(-2a)} \\ &= M^0 \cdot L^0 \cdot T^0\end{aligned}$$

where

$$\begin{aligned}a + b &= 0 \\ -2b + c + d &= 0 \\ -2a &= 0\end{aligned}$$

By solving the above simultaneous equations, we have:

$$a = 0$$

$$b = 0$$

$$c = -d$$

Let  $c = 1$ , so

$$a = 0$$

$$b = 0$$

$$c = 1$$

$$d = -1$$

Therefore,  $\pi_{11} = d/a$

11  $\pi$ 's were found:

$$\pi_1 = (\gamma d) / m$$

$$\pi_2 = (Td^2) / D$$

$$\pi_3 = T / (Pd)$$

$$\pi_4 = d / L$$

$$\pi_5 = (Td^2) / (\gamma Q^2)$$

$$\pi_6 = (\rho d) / \gamma$$

$$\pi_7 = (Td^2) / (\gamma v^2)$$

$$\pi_8 = d / \lambda$$

$$\pi_9 = (\gamma U^2) / T$$

$$\pi_{10} = (\gamma d^2 f) / T$$

$$\pi_{11} = d / a$$

Though there are so many nondimensional parameters were found, only tension parameter  $T/Pd$  and length parameter  $L/d$  have been used in data analysis until now. It



seems that the frequency increases when the tension parameter  $T/Pd$  increases under any condition. The frequency also increases when the length parameter  $L/d$  increases. The other parameters are not been used, but could be used in future studies.

## CHAPTER VI

### SUMMARY AND CONCLUSIONS

The dynamic instability characteristics of a non-moving web at air turning bars were studied. Two types of air turning bars were used: one with two rows of holes and the other with multiple rows of holes. Three types of out-of-plane instabilities were observed. The effects of the web tension, length, pressure and air leakage on the free span flutter were examined. A traveling wave theory related to current study was reviewed and nondimensional parameters were determined by using *Buckingham  $\pi$  Theorem*.

The following conclusions were obtained from this study:

1. Types of dynamic instabilities at air turning bars:
  - Out-of-phase flutter-- it occurs only when the outer row of the holes is located near the tangential line of the web.
  - In-phase flutter.
  - Free-span flutter--it may be caused by parallel channel flow, diverging channel flow, or wall jet impingement.

2. Types of static instabilities:
  - Touching of the web to the air turning bar--it occurs due to either excessive web tension or insufficient air pressure.
  - Bulging of the web--it occurs when the web tension is too low or the air pressure is too high.
3. Effect of web tension. Frequency increases when tension increases. There is a narrow range of web tension where large amplitude occurs.
4. Effect of supply pressure. Small pressure variation do not affect the frequency of free span flutter.
5. Effect of free span length of web. Frequency increases when the length of web increases. Flutter modes change when the length changes. The flutter of longer span has more nodes, and the flutter of short span can be mixed with several modes and is very complicated.
6. Effect of edge air leakage. Web flutter becomes more violent when the edge gap distance between the edge of web and side plate is smaller than a certain value. This suggests that wide webs have more flutter problems. Flutter frequency and mode also change when the edge gap is changed.
7. Effect of wrap angle. The most significant factor appears to be wrap angle  $\theta$  ( $\alpha$ - $\beta$ ), the angle between the web and a tangent to the bar at the last row of holes. Wrap angle is a very influential factor especially when the edge air leakage is very small.

## REFERENCES

- Aidun, C.,K., "Principles of Hydrodynamic Instability: Application in Coating Systems, Part I: Background", Tappi Journal, February 1991, pp. 213-219.
- Aidun, C.,K., "Principles of Hydrodynamic Instability: Application in Coating Systems, Part II: Examples of Flow Instability", Tappi Journal, March 1991, pp. 213-220.
- Banks, D.W., "Aerodynamics in Ground Effect and Predicted Landing Ground Roll of A Fighter Configuration with A Secondary-Nozzle Thrust Reverser", National Aeronautics and Space Administration, Technical Paper 2834, 1988.
- Blevins, R.D., "Flow Induced Vibration", Van Nostrand Reinhold, N.Y., Second Edition, 1990, pp.246-252.
- Chang, Y.B., "An Experimental and Analytical Study of Web Flutter", Ph.D. Dissertation, Oklahoma State University, 1990.
- Fraser, W.A.R., "Air Flotation Systems: Theoretical Considerations & Practical Applications, Part II", Paper, Film, & Foil Converter, June 1983, pp. 112-118.
- Moretti, P.M., "Multistable Flows", Invited Presentation to TAPPI Panel on Flow Instability, 1990 Engineering Conference, Seattle, WA, September 24-27, 1990.
- Pramila, A., "Sheet Flutter and the Interaction between Sheet and Air", Tappi Journal, July 1986, pp. 70-74.
- Pramila, A., "Author's Reply: Any Extended Form of Hamilton's Principle Can Be Applied to Non-conservative Straight Fluid-Pipe Systems", Journal of Sound and Vibration, Vol. 152 (3), 1992, pp. 564-566.
- Purdue, D., "Lateral Stability Investigation of Air Bar and Web Interaction for Use in Flotation Ovens", MS Thesis, Oklahoma State University, 1993
- Sundararajan, V., "Stability of Flexible Nozzle Structures", Ph.D. Dissertation, University of Kansas, 1966.

- Segawa, Y., "Analysis of the Destabilizing Effect of a Rigid Wall on the Elastic One-Dimensional Flat Plate Placed in Irrotational Flow Adjoining the Rigid Wall", JSME International Journal, Series B, Vol. 36, No. 1, 1993, pp. 26-33.
- Weaver, D.S., Adubi, F.A., and Kouwen, N., "Flow Induced Vibrations of a Hydraulic Valve and their Elimination", ASME Journal of Fluids Engineering, 1978, Vol. 100, pp. 239-245.
- Weaver, D.S., Kouwen, N., and Mansour, W.M., "On the Hydroelastic Vibration of a Swing Check Valve", Flow-Induced Structural Vibrations, August 14-16, 1972, Karlsruhe, Germany, pp. 333-338.
- Weaver, D.S., "Flow Induced Vibrations in Valves Operating at Small Openings", Practical Experiences with Flow Induced Vibrations, IAHR / IUTAM symposium, Karlsruhe, Editors, E. Naudasher and D. Rockwell, 1979, pp. 305-319.
- Zeelani, S.A.A., "An Experimental Study of Oscillatory Instability of Webs at Air Turning Bars", MS report, MAE Dept., Oklahoma State University, 1994.

## APPENDIX: TRAVELING WAVE ANALYSIS

Following an analysis by Y.B.Chang, the deflection of the membrane is assumed to be

$$w(x, t) = \text{Re}\left[Ae^{ik(x-ct)}\right]$$

where  $k = 2\pi/\lambda$  is the wave number. The linearized equation for the velocity potential is

$$\nabla^2 \phi - \frac{1}{a^2} \left( \frac{\partial}{\partial t} + U_{air} \frac{\partial}{\partial x} \right)^2 \phi = 0$$

$$\nabla^2 \phi - M^2 \left( \frac{1}{U_{air}} \frac{\partial}{\partial t} + \frac{\partial}{\partial x} \right)^2 \phi = 0$$

The flow boundary conditions are

$$\left. \frac{\partial \phi}{\partial z} \right|_{z=0} = U_{air} \frac{\partial w}{\partial x} + \frac{\partial w}{\partial t}$$

$$\left. \frac{\partial \phi}{\partial z} \right|_{z=-h} = 0$$

Assume

$$\phi = \text{Re}\left[f(z)e^{ik(x-ct)}\right]$$

Combining equations

$$\text{Re}\left[\frac{d^2 f}{dz^2} e^{ik(x-ct)} - k^2 f e^{ik(x-ct)}\right] = 0$$

that is

$$\frac{d^2 f}{dz^2} - k^2 f = 0$$

The solution is

$$f = C_1 e^{kz} + C_2 e^{-kz}$$

Therefore, the velocity potential becomes

$$\phi = \text{Re} \left[ C_1 e^{kz} + C_2 e^{-kz} \right] e^{ik(x-ct)}$$

From the first boundary condition,

$$C_1 - C_2 = iA(U_{air} - c)$$

From the second boundary condition

$$C_1 e^{-kh} - C_2 e^{kh} = 0$$

or

$$C_1 = C_2 e^{2kh}$$

Solving these equations

$$C_2 = \frac{iA(U_{air} - c)}{e^{2kh} - 1}$$

and

$$C_1 = \frac{iA(U_{air} - c)e^{2kh}}{e^{2kh} - 1}$$

Therefore,

$$\phi = \text{Re} \left[ e^{2kh+kz} + e^{-kz} \right] \frac{iA(U_{air} - c)}{e^{2kh} - 1} e^{ik(x-ct)}$$

The perturbation pressure is

$$p = -\rho \left[ U_{air} \frac{\partial \phi}{\partial x} + \frac{\partial \phi}{\partial t} \right]_{z=0}$$

Taking derivatives of  $\phi$

$$\left. \frac{\partial \phi}{\partial x} \right|_{z=0} = -Re \left[ kA(U_{air} - c) \frac{e^{2kh} + 1}{e^{2kh} - 1} e^{ik(x-ct)} \right]$$

and

$$\left. \frac{\partial \phi}{\partial t} \right|_{z=0} = Re \left[ ckA(U_{air} - c) \frac{e^{2kh} + 1}{e^{2kh} - 1} e^{ik(x-ct)} \right]$$

Therefore, equation becomes

$$p = Re \left[ \rho kA(U_{air} - c)^2 \beta e^{ik(x-ct)} \right]$$

where

$$\beta = \frac{e^{2kh} + 1}{e^{2kh} - 1} = \frac{1}{\tanh(kh)}$$

The equation of motion of the membrane is

$$\begin{aligned} & m \left( \frac{\partial^2 w}{\partial t^2} + 2U_{web} \frac{\partial^2 w}{\partial t \partial x} + U_{web}^2 \frac{\partial^2 w}{\partial x^2} \right) - \left( T_x \frac{\partial^2 w}{\partial x^2} + 2T_{xy} \frac{\partial^2 w}{\partial x \partial y} + T_y \frac{\partial^2 w}{\partial y^2} \right) \\ & + \left( D_x \frac{\partial^4 w}{\partial x^4} + 2D_{xy} \frac{\partial^4 w}{\partial x^2 \partial y^2} + D_y \frac{\partial^4 w}{\partial y^4} \right) + p_+ - p_- = 0 \end{aligned}$$

where

$$D_x = \frac{E_x h^3}{12(1 - \nu_x \nu_y)}$$

$$D_y = \frac{E_y h^3}{12(1 - \nu_x \nu_y)}$$

$$D_{xy} = D_x \nu_y + \frac{Gh^3}{6}$$

$$m \frac{\partial^2 w}{\partial t^2} - T \frac{\partial^2 w}{\partial x^2} + D \frac{\partial^4 w}{\partial x^4} - p = 0$$

$$w(x, t) = Re \left[ A e^{ik(x-ct)} \right]$$



$$\begin{aligned}
p &= \text{Re}[\rho k A (U_{air} - c)^2 \beta e^{ik(x-ct)}] \\
&- m \text{Re}[A k^2 c^2 e^{ik(x-ct)}] + T \text{Re}[A k^2 e^{ik(x-ct)}] + D \text{Re}[A k^4 e^{ik(x-ct)}] \\
&\quad - \text{Re}[\rho k A (U_{air} - c)^2 \beta e^{ik(x-ct)}] = 0
\end{aligned}$$

$$-m k c^2 + T k + D k^3 - \rho (U_{air} - c)^2 \beta = 0$$

$$\begin{aligned}
\left(\frac{c}{U_{air}}\right)^2 - \frac{T}{m U_{air}^2} - \frac{D k^2}{m U_{air}^2} + \left(1 - \frac{c}{U_{air}}\right)^2 \frac{\rho \beta}{m k} &= 0 \\
\left(1 + \frac{\rho \beta}{m k}\right) \left(\frac{c}{U_{air}}\right)^2 - 2 \frac{\rho \beta}{m k} \left(\frac{c}{U_{air}}\right) - \left(\frac{T}{m U_{air}^2} + \frac{D k^2}{m U_{air}^2} - \frac{\rho \beta}{m k}\right) &= 0
\end{aligned}$$

$$(1 + \mu \beta) \zeta^2 - 2 \mu \beta \zeta - (\tau + \delta - \mu \beta) = 0$$

where

$$\begin{aligned}
\mu &= \frac{\rho}{m k} \\
\zeta &= \frac{c}{U} \\
\tau &= \frac{T}{m U^2} \\
\delta &= \frac{D k^2}{m U^2}
\end{aligned}$$

By solving for  $\zeta$ ,

$$\zeta = \frac{\mu \beta \pm \sqrt{(1 + \mu \beta)(\tau + \delta) - \mu \beta}}{1 + \mu \beta}$$

The stability criterion is obtained by letting the discriminant be zero

$$(1 + \mu \beta)(\tau + \delta) - \mu \beta = 0$$

$$\tau + \delta = \frac{\mu \beta}{1 + \mu \beta}$$

$$\frac{T}{m U^2} + \frac{D k^2}{m U^2} = \frac{\frac{\rho}{m k}}{\frac{\rho}{m k} + \tanh(kh)}$$

$$\rho U^2 = \left( \frac{T + Dk^2}{m} \right) (\rho + mk \tanh(kh))$$

$$\rho U^2 = \left( \frac{T + Dk^2}{m} \right) \left( \rho + \frac{2\pi n}{\lambda} \tanh\left(\frac{2\pi h}{\lambda}\right) \right)$$

$$U^2 = \frac{T + Dk^2}{m} \left( 1 + \frac{2\pi n}{\rho\lambda} \tanh\left(\frac{2\pi h}{\lambda}\right) \right)$$

$$\frac{mU^2}{T} = \left( 1 + \frac{4\pi^2 D}{T\lambda^2} \right) \left( 1 + \frac{2\pi n}{\rho\lambda} \tanh\left(\frac{2\pi h}{\lambda}\right) \right)$$

$$U^2 = \frac{T}{m} \left( 1 + \frac{4\pi^2 D}{T\lambda^2} \right) \left( 1 + \frac{2\pi n}{\rho\lambda} \tanh\left(\frac{2\pi h}{\lambda}\right) \right)$$

$$U^2 = \frac{4\pi^2 D}{m\lambda^2} \left( 1 + \frac{2\pi n}{\rho\lambda} \tanh\left(\frac{2\pi h}{\lambda}\right) \right)$$


$$\frac{mU_{crit}^2}{T} = 1 + \frac{2\pi n}{\rho\lambda} \tanh\left(\frac{2\pi h}{\lambda}\right)$$

The critical flow velocity monotonically increases with the spacing between the membrane and the wall, and decreases with the increase of wavelength. When  $\lambda/h \rightarrow \infty$ , the critical flow velocity converges to its minimum value, which is

$$\left. \frac{mU_{crit}^2}{T} \right|_{min} = 1$$

If the wavelength is small, that is  $\lambda/h < 2$ , the critical flow speed reaches its maximum value and does not change with  $\lambda/h$ .

$$\left. \frac{mU_{crit}^2}{T} \right|_{max} = 1 + \frac{2\pi n}{\rho\lambda}$$

VITA 

Linda Lei Chen

Candidate for the Degree of

Master of Science

Thesis: DYNAMIC INSTABILITY AND "BUZZ" AT AIR TURNING  
BARS

Major Field: Mechanical Engineering

Biographical:

Personal Data: Born in Shanghai, China, on October 22, 1968, the daughter of  
Mr. Xiao-Wei Chen and Mrs. De-An Zhang Chen.

Education: Received Bachelor of Science degree in Shanghai from China  
Textile University in July, 1991.  
Completed the requirements for the Master of Science degree with a  
major in Mechanical Engineering at Oklahoma State University in  
May, 1996.

Professional Experience: Mechanical Engineer, Shanghai Kohden Medical  
Electronic Instrument Corp., 1991-1993; Operation Engineer, ALCATEL  
Bell Telephone. Comp. Shanghai Liaison Office, 1993-1993;  
Graduate Research Assistant, School of Mechanical and Aerospace  
Engineering, Oklahoma State University, 1994-1995.